

2-8-2011

Fractal modeling of lightning

Paul Greninger

Follow this and additional works at: https://digitalrepository.unm.edu/phyc_etds

Recommended Citation

Greninger, Paul. "Fractal modeling of lightning." (2011). https://digitalrepository.unm.edu/phyc_etds/19

This Thesis is brought to you for free and open access by the Electronic Theses and Dissertations at UNM Digital Repository. It has been accepted for inclusion in Physics & Astronomy ETDs by an authorized administrator of UNM Digital Repository. For more information, please contact disc@unm.edu.

Paul Greninger

Candidate

Physics and Astronomy

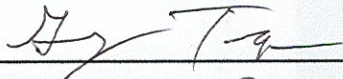
Department

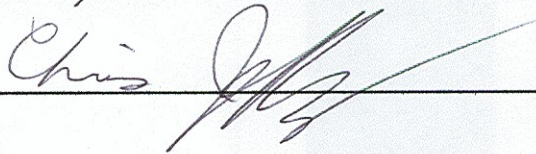
This thesis is approved, and it is acceptable in quality
and form for publication:

Approved by the Thesis Committee:



, Chairperson





Fractal Modeling of Lightning

BY

PAUL GRENINGER

MS PHYSICS UNM, 2010

MS PHYSICS NYU, 1976

BA PHYSICS SUNY BUFFALO, 1971

THESIS

Submitted in Partial Fulfillment of the
Requirements for the Degree of

MS PHYSICS

The University of New Mexico
Albuquerque, New Mexico

12/2010

I heartily acknowledge Chris Jeffery for introducing me to sprites, program R, and for valuable conversations in electromagnetic modeling.

To Christopher Watts for procuring for me the original position at Los Alamos National Laboratory.

To Mark Gilmore, and Gregory Taylor for serving on my committee.

To my wife Virginia who supported me and encouraged me.

FRACTAL MODELING OF LIGHTNING

BY

PAUL GRENINGER

ABSTRACT OF DISSERTATION

Submitted in Partial Fulfillment of the
Requirements for the Degree of Master of Science

MS Physics

The University of New Mexico
Albuquerque, New Mexico

12/2010

Fractal Modeling of Lightning

by

Paul Greninger

MS, Physics UNM, 2010

MS, Physics, NYU, 1976

BA, Physics, SUNY Buffalo, 1971

ABSTRACT

A program has been developed that portrays the fractal modeling of lightning, which subsequently calculates the fields from a fractal antenna. Nodal currents are weighted with branch length. The Hausdorff dimension for various growth parameters η , agree with those in the literature. Electric fields in the far zone have been calculated by weighting the branch currents with an overall damped sinusoidal current. The current waveform for each element is evaluated at retarded times based upon the speed the discharge propagates along the fractal. At scale lengths of 100 m an interference pattern becomes noticeable. We have investigated the slope of the power spectrum for spider lightning. For $f < f_{\text{threshold}}$ the slope is between -1.6 to -2.6 with a standard deviation of ~ 2 . In the case of channel lightning this slope would be -2. For $f > f_{\text{threshold}}$ the average slope varies between -3.4 and -3.5. In the case of channel lightning this slope would be -4. The lesser slope is attributed to more interference between radiating elements in this model. For $f > f_{\text{threshold}}$ the slope appears to be independent of the growth parameter η . Observations show for inter-cloud lightning the threshold frequency is 50 kHz, with zero slope for $f < f_{\text{Thresold}}$ and -1.6 slope for $f > f_{\text{Thresold}}$.

12/2010

Table of Contents

ABSTRACT	v
Table of Figures.....	vii
Nomenclature.....	viii
1. Introduction	1
2. Idea of a Fractal	9
3. Properties of a Fractal.....	10
4. Method	12
5. Sample Output	28
6. Plotted Output	28
7. Radiated Fields	32
8. Slope of the Power Spectrum	39
9. Future Work	44
10. Conclusion.....	44
Appendix 1. Folker-Plank Equation.	
Appendix 2 Code Sample Used to Solve the Laplacian.	
Appendix 3. Identity $\int d^3x J = -i\omega \vec{P}$	
Appendix 4. How to Convert Gaussian to mks	
Appendix 5. Sample Output	
Appendix 6. How the Program Works and Summary of Subroutines	

Table of Figures

Figure 1. Electrical discharge pattern on a glass plate.....	10
Figure 2. Koch Curve. As you resolve down 3x in power the perimeter increases to 4/3 its value.	11
Figure 3. Image generated using a Mandelbrot set.	11
Figure 4. Measuring the shore line with smaller and smaller ruler the answer diverges.	12
Figure 5. Probabilities weighted with electric field.	14
Figure 6. Points are added at random to the grounded structure.	14
Figure 7. 5000 points plotted where the growth parameter $\eta=0$. This corresponds to cancer growth.	16
Figure 8. 5000 points plotted where the growth parameter $\eta=0.5$	17
Figure 9. 5000 points plotted growth parameter $\eta=1.0$. The probabilities are linear weighted with potential and Hausdorff dimension = 1.75	18
Figure 10. 1985 points plotted where the growth parameter $\eta=2$. A more spindly pattern emerges.	19
Figure 11. Hausdorff dimension vs. growth factor η	21
Figure 12. Current distribution assumed throughout the fractal.	22
Figure 13. Weighting fractal branches with path length.	26
Figure 14. Flow chart of code.....	27
Figure 15. Fractal 1, 1000 points. Graphical validation of current weighted with path length.	29
Figure 16. Fractal 2, 1000 points. Graphical validation of current weighted with path length.	30
Figure 17. Fractal 3, 1000 points. Graphical validation of current weighted with path length.	31
Figure 18. Magnitude of electric field, vertical and horizontal components, with Fourier transform. At grid = 1 m it acts just as an antenna where frequencies taper off smoothly above 10 kHz.	36
Figure 19. Magnitude of electric field, vertical and horizontal components, with Fourier transform. At grid = 10 m some fractal noise begins to appear above 10 kHz.....	37
Figure 20. Magnitude of electric field, vertical and horizontal components, with Fourier transform. At grid = 100 m substantial fractal noise becomes apparent above 10 kHz.	38
Figure 21. Slope of the EV power spectrum $f < f_{\text{threshold}}$ slope=2.5 and $f > f_{\text{threshold}}$ slope=3.5 . Triangle at bottom abscissa is where $f_{\text{threshold}}$ is.....	40
Figure 22. Slope of the EH power spectrum $f < f_{\text{threshold}}$ slope=2.4 and $f > f_{\text{threshold}}$ slope=3.6 . Triangle at bottom abscissa is where $f_{\text{threshold}}$ is.....	41
Figure 23. Average slope of EV $f < f_{\text{threshold}}$ and $f > f_{\text{threshold}}$ (n=50). Error bars denote standard deviation over 50 runs each.....	42
Figure 24. Average slope of EH $f < f_{\text{threshold}}$ and $f > f_{\text{threshold}}$ (n=50). Error bars denote standard deviation over 50 runs each.....	43

Nomenclature

A	a constant
α	decay constant
β	velocity divided by speed of light
c	speed of light
∇^2	Laplacian operator
E	electric field
\vec{E}_{rad}	electric field in the radiation zone
γ	rise time constant
H	horizontal component
$H(t)$	Heavyside step function
i	index along the abscissa
I, I_0, I_l	a current
J	current density
i	$\sqrt{-1}$ (where appropriate)
j	index along the ordinate
k	free space wave vector
\hat{L}_n	orientation of the n^{th} element
L	independent scale length
η	an exponent to the electric field, used to vary the probability
N	number of points
\vec{n}	unit normal from the observation point to the source
n	density of points
n_f	number of oscillations in decay time $1/\alpha$
ν	collision frequency
\vec{P}_\perp	electric dipole moment perpendicular to normal of observation
$p(i,j)$	probability at point i, j
ϕ	potential at a point
$\phi(i, j)$	potential of $i^{\text{th}}, j^{\text{th}}$ coordinate along the grounded structure
$\phi(i', j')$	potential of $i^{\text{th}}, j^{\text{th}}$ coordinate of ungrounded neighbor
s_n	path along the n^{th} element of fractal
r_n	vector to the n^{th} element
r	radius
t	time
τ	a retarded time
$\vec{\theta}$	vector direction in the azimuthal direction
μ_0	susceptibility of free space
V	vertical component
v	velocity of propagation
ν_{ion}	ion production rate
ω	an angular frequency

\vec{x}
 x, y, z observation point
coordinate in space

1. Introduction

1.1. What is a Sprite

High altitude sprites were detected more than 100 years ago (Kerr 1994). Sprites are transient luminous events which appear in clean air above a thunderstorm following intense lightning (Pasko, Inan and Bell 2001). Upper extremities of sprites appear as an amorphous diffuse glow, while lower portions exhibit a complex streamer structure. They have been described as having a branching tree pattern, with highly localized filamentary structures (Pasko, Inan and Bell 1998). Propagating downward they reach speeds up to 10^7 m/s, and are often described as jellyfish optical flashes. Dimensions in altitude span 50-90 km, with internal dimension 5-30km. Bright red colors are in its 'head' 66-74 km, with strong blue emissions originating at their streamer tips.

Sprites are almost always associated with positive Cloud to Ground (CG) lightning (Pasko et al. 1997). Positive lightning strokes have the largest current associated with them (Uman 1987).

Sprites are comprised of three regions: 1) The 'hair', for altitudes greater than 85 km. This region is characterized by collective multiplication of electrons, and diffuse terminations of branches on the lower ionosphere. Here can be seen the evolution of the discharge tree into hot spots (Pasko et al. 2002), 2) The 'head' is located at altitudes 75-85 km. This region is characterized by strong attachment of ambient electrons before Electrical Breakdown (EB), 3) The lower region, streamers, are at altitudes below 75 km. Here there is strong attachment and individual electron avalanches. Tendrils of decreasing intensity extend down to cloud tops.

1.2. Lightning Phenomenology

Lightning is measured in terms of kA (Uman 1987). Well over half of all lightning is Inter-Cloud (IC). Of the remainder, 90% is -Cloud to Ground (-CG). In -CG there is a downward negative charged leader. Only in 10% of the remainder, +CG, is a positive charged leader.

Negative CG lightning could bring to earth a total charge of up to 10C. A total discharge is called a flash, it occurs in about 0.5 s. A flash is made up of several components. Three-to four current pulses are called a stroke. Each stroke lasts about a millisecond. The time between strokes typically lasts 10 ms. They appear to flicker because the eye can just resolve individual pulses in a stroke.

A stepped leader process is believed to be initiated by breakdown within the cloud. It continues down to earth, where it attaches itself to the earth. Then a return stroke follows, positive up from the ground through the previously ionized channel. This travels approximately one-third the speed of light and typically carries 30 kA. Currents fall to one-half their value in 50 μ s. The return stroke heats the leader channel to 30,000 °K. This in turn generates a high pressure shock wave. Additional charge may flow from the cloud top through a dart leader.

There are two theories on the build up of a cloud dipole charge. The first is a precipitation theory, while the second is a convection theory. In the precipitation theory falling particles interact with lighter particles carried in an updraft. An interaction process charges the heavier particles negative. These particles are at an approximate -5 °C temperature. Lighter particles are charged positive. Gravity and updrafts separates them to form opposite charges in a dipole. Negative charge resides at the bottom, while positive charge resides at the cloud top. Particles may also charge by induction. In the convection process charges accumulate near the earth's surface or across regions of varying air and cloud conductivity.

1.3. Three Schools of Thought

EB associated with sprites starts in the atmosphere above thunderstorms where the local fields exceed the breakdown field (Pasko et al. 1998) There are three schools of thought. The first is quasi-static model based upon thundercloud electromagnetic fields (QE). The second is heating by lightning induced electromagnetic pulses (Taranenko, Inan and Bell 1993a). The third is runaway electron avalanches driven by the QE fields. In the QE model (Pasko et al. 1997) fields are set up as a result of storing and moving 200C in 1ms.

There is an associated conduction current $J = \sigma \cdot E$. The heating mechanism proceeds as follows. Increasing in altitude the electron mobility increases, whereby conductivity increases. The induced currents from electric fields increase. These currents cause increased heating of ambient electrons, which in turn modifies the conductivity. The field penetration and relaxation are all solved in a self-consistent manner.

The EMP model is a low frequency model of electrical breakdown (Milikh, Papadopoulos and Chang 1995, Taranenko, Inan and Bell 1993b). In the first reference an upward propagating electromagnetic pulse is generated by a horizontal lightning strike. In the second reference an upward RF pulse is launched with a waveform of duration 100 μ s. The second reference cites the critical parameter as the quiver energy (see Appendix 1) for pulses longer than the reciprocal of the electron-neutral collision frequency. It is the electron kinetic energy of this charged particle in an oscillating electric field. For the quiver energy less than 0.1 eV the electron energy results in optical emission. For greater values breakdown occurs.

In the run away electron avalanche model electrons rapidly pick up speed in an electric field. The mean free path at 100 km is approximately 1 meter (Taranenko et al. 1993a). Hence an E field of 20 V/m would produce 20 eV. These are ionization energies. Collisions with other particles create even more particles.

In comparison, Bell states that the EMP model (Taranenko et al. 1993a) gives red emissions in the first positive band of N_2 at a peak of 80-95 km, while red sprites are observed at 66-74 km (Bell, Pasko and Inan 1995). The QE model (Pasko et al. 1997) has been criticized as having the presence of unrealistic charges (Valdivia, Milikh and Papadopoulos 1998). Cheng (Cheng et al. 2007) relates lightning with observations of D region perturbations. The same stroke produced an Elve, which are known to be EMP related. His conclusion was the particular lightning analyzed has an EMP effect.

1.4. Model of Red Sprite

Stanford University has a model of a red sprite (Pasko, Inan and Bell 2000). Breakdown voltage is when the ionization rate for ions is approximately equal to attachment rate for electrons. Raiser states that the limit for positive breakdown streamer voltage is less than that for negative voltage (Raiser 1997). This is because electron avalanches once started near an anode enter a region of only higher field gradient. In this model positive charge is removed by a positive CG lightning strike (positive charge being placed at the ground). Positive streamers go up while negative streamers go down. In this fashion different breakdown criteria are stored in the model. The mean free path increases at higher altitude where it is easier to break down. Let E_k^+ be the positive critical field for breakdown. Similarly let E_k^- be the negative critical field for breakdown. Quantities E_k^+ and E_k^- scale with altitude. Their model works as follows. Growth of a single discharge tree is initiated by a single electron avalanche. The potential of this point is fixed. The discharge pattern is propagated by adding links. Only one link is added at any time step. Fields are calculated on the entire grid after each step. Each link has a probability proportional to the difference of its field less the critical breakdown field. Based upon probabilities a new random choice is made and a new step realized. The result is that the model qualitatively gives some realistic looking 'jellyfish' sprites. Quantitatively, the lowest stopping altitude agrees well with the stopping altitude for positive streamers.

There is also a 3-D model. Slightly higher fields as calculated, since the corona is modeled as true channels (Pasko et al. 2001).

1.5. Valdivia Paper and Model

We shall be largely following Valdivia's paper (Valdivia et al. 1998) and include some salient features. They developed a model that did away with unrealistically large charges in the QE model. Another draw back of the QE model is the fields smoothly dissipate at ionospheric heights, failing to account for the spatial structure of red sprites. Valdivia's model takes into account the

calculation of transient fields. They find that the model leads to more natural observations of red sprite structure, and significantly reducing the required threshold charge. This model includes the structuring of emission. Here fields interact and energize ambient electrons, generating non Maxwellian distribution functions. The collision of energetic electrons with neutral particles results in observed emissions.

In the Valdivia model (Valdivia et al. 1998) a fractal antenna generates a spatially non-uniform radiation pattern. We can define a fractal antenna if we run currents through a fractal pattern. These gain patterns can reduce the lightning energy compared to that of a dipole. The antenna has a non-uniform distribution of radiation elements, which contribute to the radiated power. The strength and orientation of individual elements is represented by a vector. There is a phase that relates to the spatial distribution of elements. For random phase the gain scales as the number of elements. For perfect coherent phase the gain scales as the number of elements squared. Partial coherence lies in between these two limits. The spatial distribution depends upon a fractal dimension. Valdivia et al. first considers the case of channel lightning. Channel lightning resides in a single channel and zig zags back and forth in 2D. The tortuous model increases the number of radiating elements compared to that of a dipole. The line elements will add constructively at certain points and destructively at other points. Valdivia et al. found a clear increase in the array factor, up to ten fold, which contributes to the gain of the antenna. Mathematically the gain above that of a single dipole had an additive term containing a multiple of increased path length and a differential in time that the pulse takes to propagate along the fractal.

Next Valdivia develops a model of inter-cloud lightning model with multiple branches. Following Niemeyer (Niemeyer, Pietronero and Wiesmann 1984) this model naturally leads to a fractal pattern. The fractal dimension can be easily parameterized by a parameter η . They generate a fractal tree pattern where the higher the value of η the less probability there is to branch. The probability of not changing direction goes as the electric field raised to the power η . Next they run currents along the dendritic arms. The fields propagate to the D region where

they generate a highly non-Maxwellian distribution, which increases the number of electrons-neutral collisions. The electron energization is computed with the help of a Folker-Plank Equation. The kinematic treatment will provide the collision frequency as function of the height and the electric field. The ambient collision frequency is found by numerically solving the Folker-Plank equation. They found for a quiver energy between 0.02 and 0.1 eV, optical emissions exist, and for values over 0.1 eV, break down occurs. Next they looked at excitation of $N_2(1P)$ states of diatomic nitrogen and the resultant optical emissions. Valdivia computes 100 kR of radiation for a current of 200 kA. He states these are reasonable values. He finds spatial distributions over 100 km in the horizontal dimension as observed at a height of 90 km. He then shows for different values of $\eta=1, 2, \infty$ and fixing the light output at 100 kR other spatial distributions exist in the horizontal dimension x . Fixing the current at 100 kA he shows the most light output for the fractal dimension $D=1.25$.

1.6. Why The Valdivia Model?

Horizontal discharges with dimension 100 km have been observed with +CG (Valdivia et al. 1998). Red sprites seem to be uniquely correlated with +CG. For fields to get projected upward discharges in a horizontal plane are the optimal configuration. This model tries to account for the dendritic fine structure by structuring emissions to highly inhomogeneous field projected into the lower ionosphere. Other models such as run away electrons are not as well documented.

1.7. Fractal Statistics

Why a fractal model? Mandelbrot states that lightning does not travel in a straight line (Mandelbrot 1982). In a fractal the degree of irregularity is identical at all scales. The fractal trees of the Peano curve are good 1st order models of river sheds, botanical trees and human vascular systems. Niemeyer analyzed a discharge pattern and found the fractal dimension $D=1.75$ (Niemeyer et al. 1984). Stochastic models look the same as a discharge. The model naturally leads to a fractal structure. Vecchi states, "the radiated field is a fractal in itself (Vecchi, Labate and Canavero 1994)." For channel lightning, "the radiated field appears

to have the same dimension as the channel.” Lightning is considered a collective phenomenon, where the important aspect of its behavior has little to do with the exact microscopic details (Gou et al. 2009). An example of fractal modeling would be modeling of a shore line with a Koch curve. As one resolves down $1/3$ in size the perimeter increases to $4/3$ its previous value. This is analogous to measuring the shore line with progressively smaller and smaller a ruler. The answer diverges!

The number of points or length of curve is expressed by $N \propto r^D$, where D the fractal dimension need not be an integer. The density of points is given by the relation $n(r) \propto r^{D-1}$. Fractal dimensions only hold on a scale larger than the average length between nodes.

Valdivia states the gain of a fractal antenna (Valdivia et al. 1998). There is an incoherent term $G \propto N$, where N is the number of elements. There is also a coherent term $G \propto N^2$. Vecchi also provides a threshold time for a single-channel-model of lightning (Vecchi et al. 1994). Let L be the scale length of the model, and v the velocity of propagation. The time constant τ is defined as

$\tau = \frac{L}{v}$. For *frequencies* $< \frac{1}{2\tau}$ the power spectrum $\propto \frac{1}{f^2}$, and the channel

behaviors as a tortuous channel. For *frequencies* $> \frac{1}{2\tau}$ the power spectrum $\propto \frac{1}{f^4}$,

and the channel behaves as a straight line. The same time constant also appears in the frequency domain. The time lag between successive arrivals is proportional to L , the scale length. For small L we expect the field time waveform to be smooth. For large L we expect to see some fractal characteristics in the radiated fields.

1.8. Ionization

Because of the Maxwellian tail there are particles reduced in number, but still moving with speeds greater than the average energy. Hence, it is not necessary that the average energy exceed the ionization energy for ionization. The presence of an electric field creates a highly non-Maxwellian distribution function. There is an increased number of electron-neutral collisions. This may be

calculated with the help of a Folker-Plank code (Tsang et al. 1991)(Appendix 1). Electrical breakdown occurs when the ion production rate is approximately equal to the attachment rate. Ionization produces electrons, while attachment takes away electrons. This last equation is expressed as $O_2 + e \rightarrow O^- + O$. The ions are viewed as too stationary to conduct. The electron production rate equals the ionization rate minus the attachment rate. Ionization rates are given by (Papadopoulos et al. 1993). They are a function of the effective collision frequency + the characteristic field. In turn the characteristic field is a function of the neutral density, the effective collision frequency, and the frequency of field excitation. The attachment rate is given by Gurevich for high energy electrons in the 'tail'.(Gurevich 1977). Here the Boltzman equation is solved for the electron distribution function $f(r,v)$, where v is velocity. The dissociative attachment equation is solved in terms of the electron distribution function, electron velocity, a relevant cross section, and collision rates for N_2 , and O_2 . An increase in the electron concentration from the heating of electrons can lead to a decrease in the dissociate recombination coefficient. Ionization rates and attachment rates can be approximated by their steady state values (Taranenko et al. 1993a).

1.9. What We Don't Know About Sprites

As already mentioned there are three schools of thought : 1) the quasi static, 2) the EMP model , and 3) run away electrons. Streamer corona could be as small as 10 m requiring cm resolution. With sprites dimensions as large as 70 km this discretization would create large computational difficulties on a grid. On a macroscopic scale the physics of streamer corona should not change below a certain level of discretization. This needs to be proved. In terms of sprite morphology we don't understand their fine structure, or their clustering. Proponents of the QE model state that very little is known about the actual altitude of positive charge removal by sprite producing CG.

1.10. Radio Frequency Perturbations in the D Region

Total ion production rate is the rate of ion production less the number of

attachment. $\frac{dN_{ionization}}{dt} = \nu_{ionization} N_{ion}$

$$\frac{dN_e(x)}{dt} = \frac{dN_{ionization}}{dt} - \frac{dN_{attachment}}{dt}.$$

Assuming relatively long times for relaxation (0.5 s) this equation may be integrated directly with respect to time to find the total number of ions.

$$N_e = \int \frac{dN_e}{dt} dt$$

The plasma frequency squared is related to the total number of ions

$$\omega_p^2 = \frac{N_e e^2}{\epsilon_0 m}.$$

The index of refraction is related to the frequency of a signal propagating through the medium as (Jackson 1975)

$$n^2 = 1 - \frac{\omega_p^2}{\omega^2} \text{ If the last argument is small a Taylor expansion would yield}$$

$$n = 1 - \frac{\omega_p^2}{2\omega^2}.$$

For photons in a vacuum $f_p \rightarrow 0$, $n \rightarrow 1$

1.11. Outline of Thesis

Out of all these possible topics we now focus on the fractal modeling of spider lightning. We shall calculate some fractal statistics and then the radiated fields from a fractal antenna. Section 2 deals with the idea of a fractal. In section 3 properties of a fractal are presented. In section 4 the method to generate a fractal is introduced. Section 5 refers to sample output. Section 6 offers some plotted output. Section 7 calculates the radiated fields. Section 8 looks at the slope of the power spectrum. Section 9 mentions future work. Section 10 provides a conclusion.

2. Idea of a Fractal

As explained in the introduction with a fractal the degree of irregularity is identical at all scales. In this section we elaborate on the idea of a fractal.

A fractal is a pattern that when subdivided, each part has the same statistical character. Fractals have been used in modeling structures of eroded coast lines and snow flake patterns. There is an idea of randomness in a fractal pattern. In addition lightning possesses a Faraday cage effect. Streamers bound areas of no discharge. This is analogous to conductors sheltering an area that becomes a field free region. Below is a discharge pattern on a glass plate.

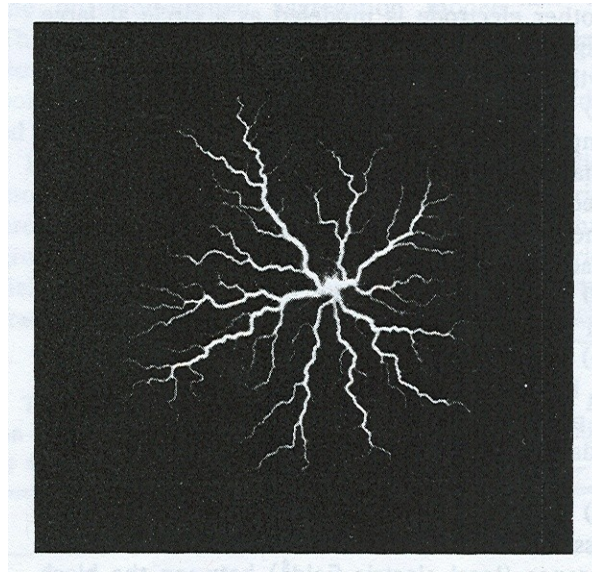


Figure 1. Electrical discharge pattern on a glass plate.

Examples of a fractal are 1) a snow flake pattern, 2) a tree divided itself into branches, 3) a leak pattern sub-divides itself into veins. It's as if nature had a random number generator. Every so often when it replicates itself, nature produces a branch.

3. Properties of a Fractal

Discussed in the introduction was the idea that fractals have dimension D that is not necessarily an integer. The number of points $N \propto r^D$, and the density of points $n(r) \propto r^{D-1}$. Also mentioned was a Koch curve, which when magnified three times in size the perimeter increases to 4/3 its previous value. See figure 2.

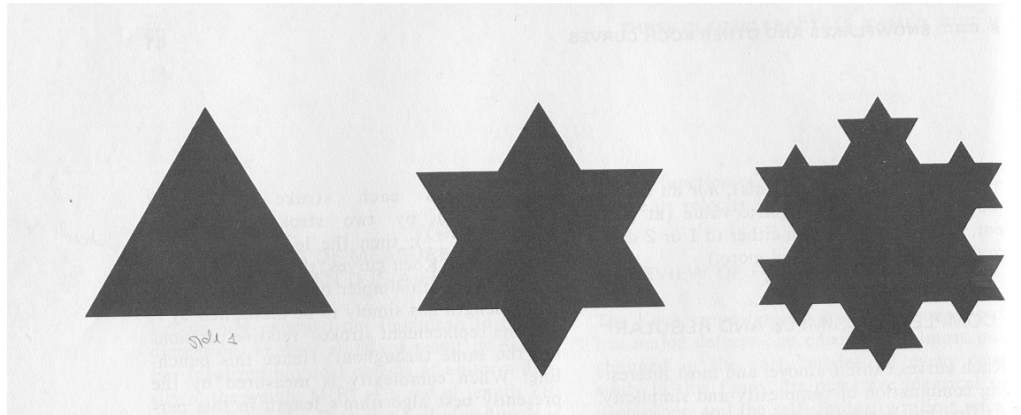


Figure 2. Koch Curve. As you resolve down 3x in power the perimeter increases to 4/3 its value.

In this section we elaborate on some properties of fractals.

Mathematically the Mandelbrot set can be defined as a bound set where

$$z_{n+1} = z_n^2 + c$$

This series is not convergent for $c=1$, but is bound for $c=i$, $i=\sqrt{-1}$. Mathematically this means that for $c=1$ z_{n+1} has no bound, while for $c=i$ z_{n+1} the set is bounded. Applying the iteration repeatedly, the modulus of z_n never exceeds a certain number, however large n gets. When computed and graphed on the complex plane, as shown in figure 3, the Mandelbrot Set is seen to have an elaborate boundary which does not simplify at any given magnification. This qualifies the boundary as a fractal.

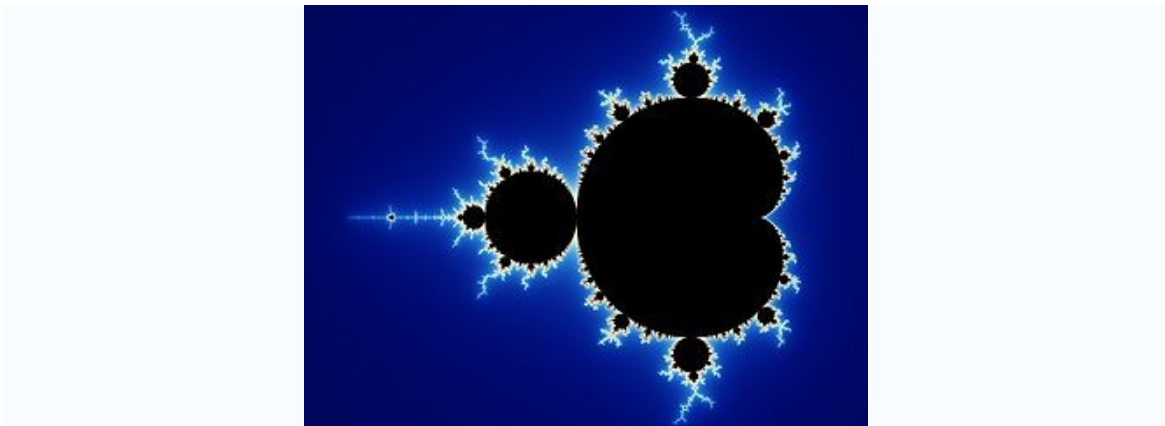


Figure 3. Image generated using a Mandelbrot set.

Another property of a fractal is when you measure the perimeter with a smaller and smaller ruler, the answer diverges. As you resolve down smaller and smaller more variability is revealed, (refer to figure 4). The answer is totally dependant upon the size of the ruler used. As the size of ruler approaches zero the length tends to infinity. In a mathematical world we can infinitely subdivide. Of course in a quantum world we would eventually hit the uncertainty principal and any further subdivision would become meaningless.



Figure 4. Measuring the shore line with smaller and smaller ruler the answer diverges.

4. Method

4.1. Stochastic Model

In this section, we follow Valdivia et al (1998) and construct a stochastic model of spider lightning. Field points are chosen at random but each time the

potential solution is recalculated. Hence the field points are laid down in a self-consistent manner.

As a starting point take a circle whose potential is set equal to unity on the outer radius. Inside the circle the center point is grounded. Laplace's equation $\nabla^2 \phi = 0$ is solved.

Laplace's equation comes about from the diffusion equation $D\nabla^2 \phi = \frac{\partial \phi}{\partial t}$. This is

a second order Differential Equation (DE). There are two boundary conditions

$\phi = 0, \frac{\partial \phi}{\partial t} = 0$. The time independent solution is desired, therefore $\nabla^2 \phi = 0$.

Proceed by expanding the potential ϕ in a power series about x .

$$\phi(x + \Delta x) = \phi(x) + \phi'(x)\Delta x + \phi''(x)\frac{\Delta x^2}{2}$$

$$\phi(x - \Delta x) = \phi(x) - \phi'(x)\Delta x + \phi''(x)\frac{\Delta x^2}{2}$$

add these two equations, $\phi'' \Rightarrow \nabla^2 \phi$

$$\nabla^2 = \frac{\phi(x + \Delta x) + \phi(x - \Delta x) - 2\phi(x)}{\Delta x^2} = 0$$

$$\Rightarrow \phi(x) = \frac{\phi(x + \Delta x) + \phi(x - \Delta x)}{2}$$

$2D :$

$$\phi(x, y) = \frac{\phi(x + \Delta x) + \phi(x - \Delta x) + \phi(y + \Delta y) + \phi(y - \Delta y)}{4}$$

The code development is done in program R. See Appendix 2 for code sample.

Now randomly add points to the grounded structure. This is analogous to the fact that if streamers move to a nearby point then this point is effectively at the same potential as the point before.

To each of these points stochastically weight the probabilities with the electric field E . Say one area has an electric field of a certain value and another area has an electric field of twice this value. Then on a scale of zero to one the area of twice the electric fields get the probability of 0.67. See figure 5 below.

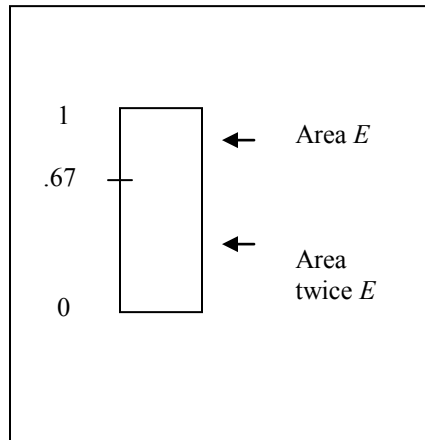


Figure 5. Probabilities weighted with electric field.

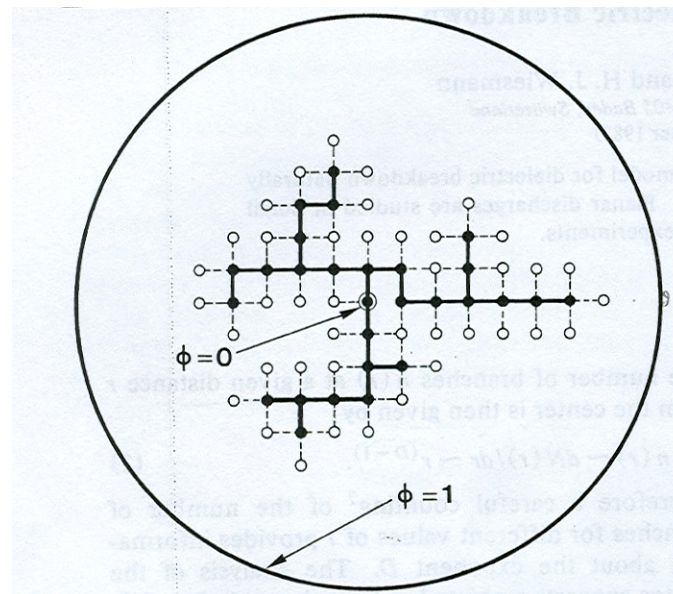


Figure 6. Points are added at random to the grounded structure.

The probability to find the next point from among the grounded neighbors proceeds as follows. Let us say in the diagram above the black grounded points have the i, j , coordinates and white neighbors have i', j' coordinates (see figure 6). Since the electric field at a grounded point is proportional to the potential of the neighbor we arrive at the following equation..

$$p(i, j) = \frac{\phi(i', j')}{\sum_{i, j} \phi(i', j')} \quad (1)$$

This is direct weighting with the electric field. A more general equation is

$$E \propto \phi \Rightarrow P \propto E^\eta$$

where P is the probability.

Different cases arise for various values of the growth parameter η .

$\eta = 0$ corresponds to cancer growth.

$\eta = 1$ probabilities are linear weighted with potential. This has a Hausdorff dimension $D = 1.75$.

$\eta = 2$ corresponds to a more spindly growth pattern.

Plots are now presented for the growth parameter $n=0, 0.5, 1, 2$ in figure 7 through figure 10.

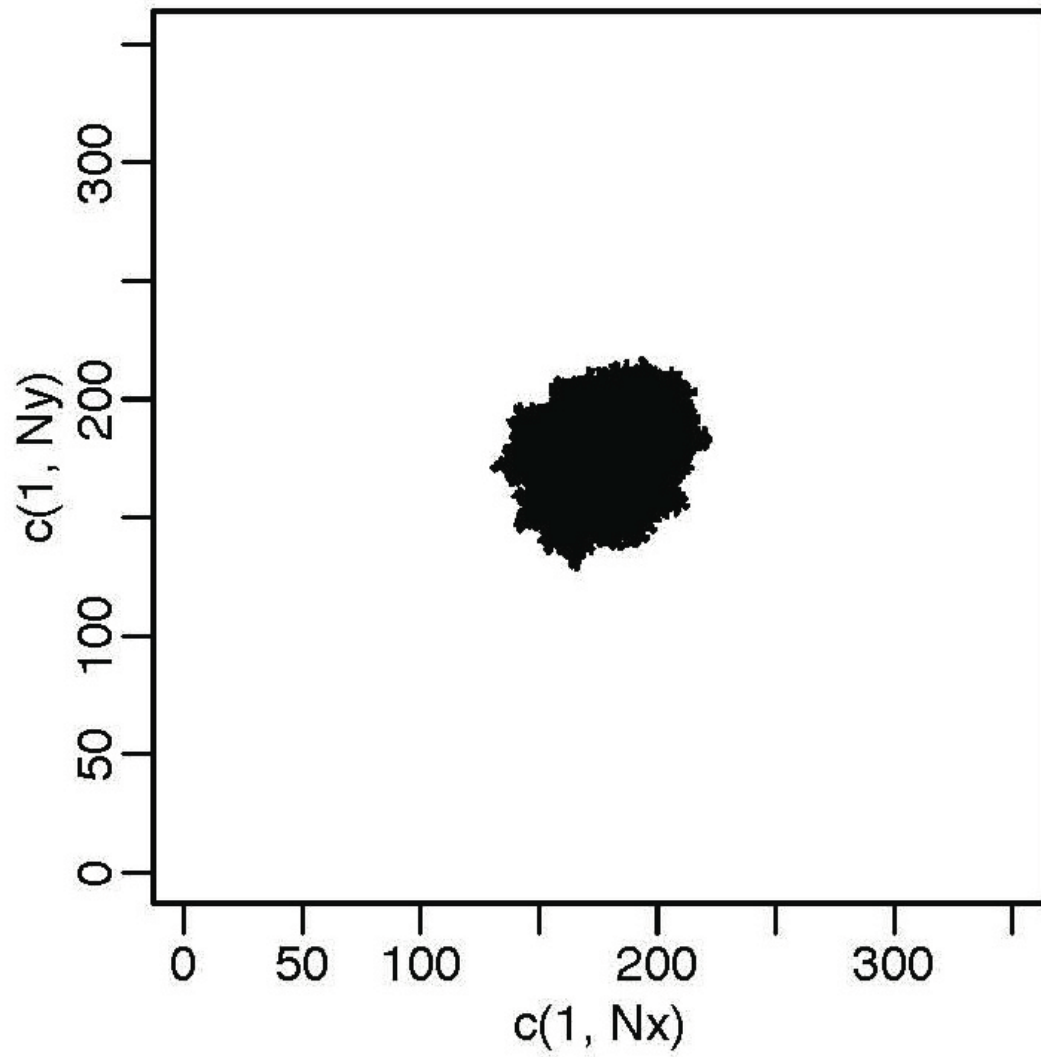


Figure 7. 5000 points plotted where the growth parameter $\eta=0$. This corresponds to cancer growth.

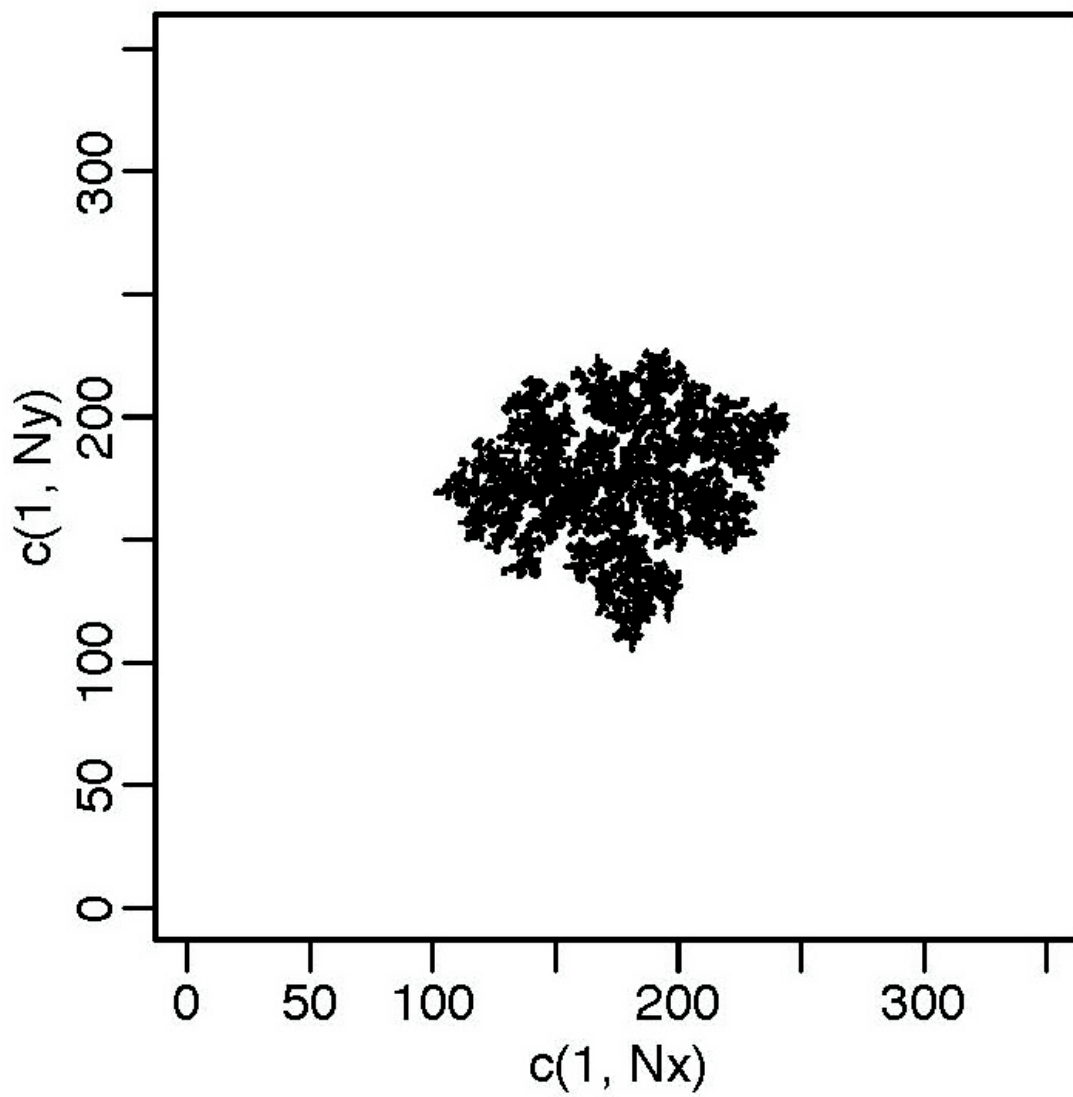


Figure 8. 5000 points plotted where the growth parameter $\eta=0.5$.

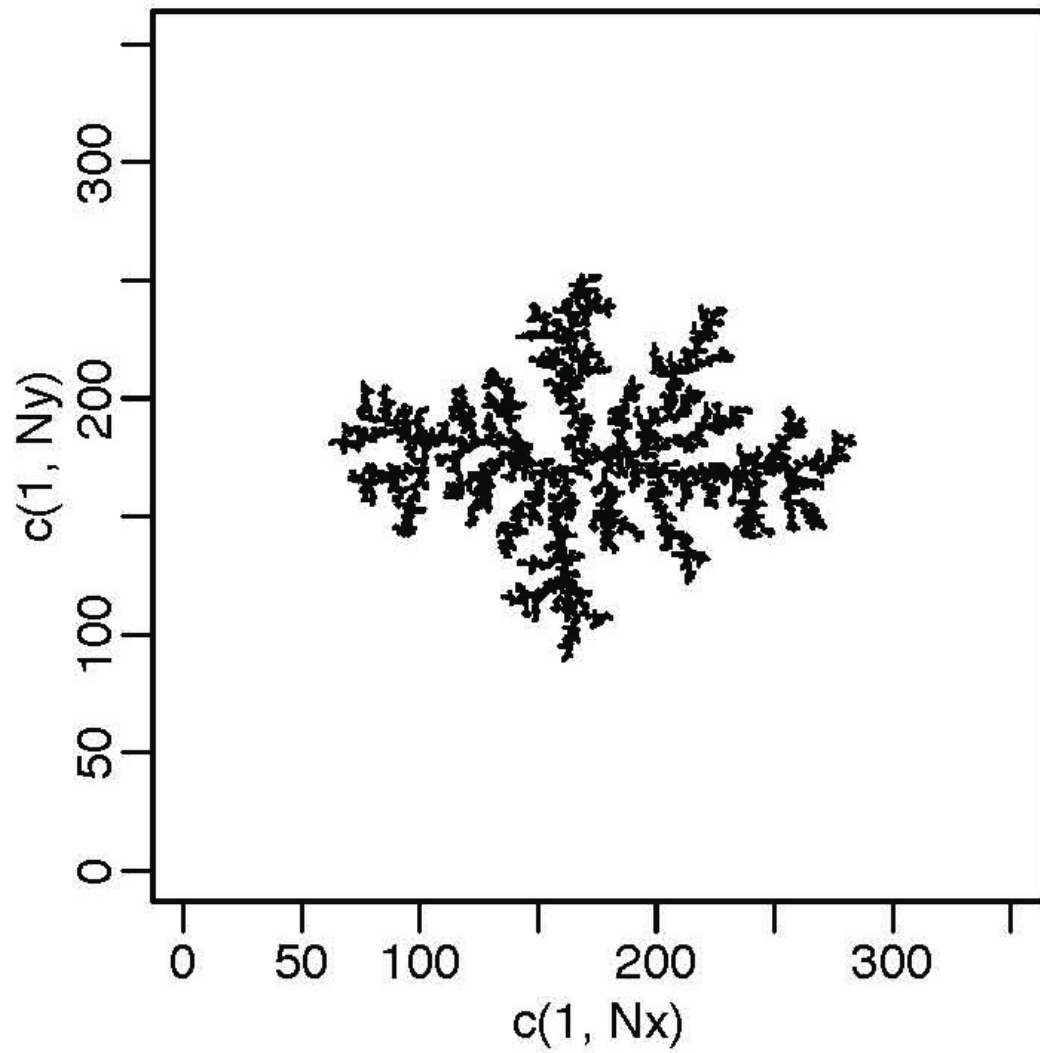


Figure 9. 5000 points plotted growth parameter $\eta=1.0$. The probabilities are linear weighted with potential and Hausdorff dimension = 1.75 .

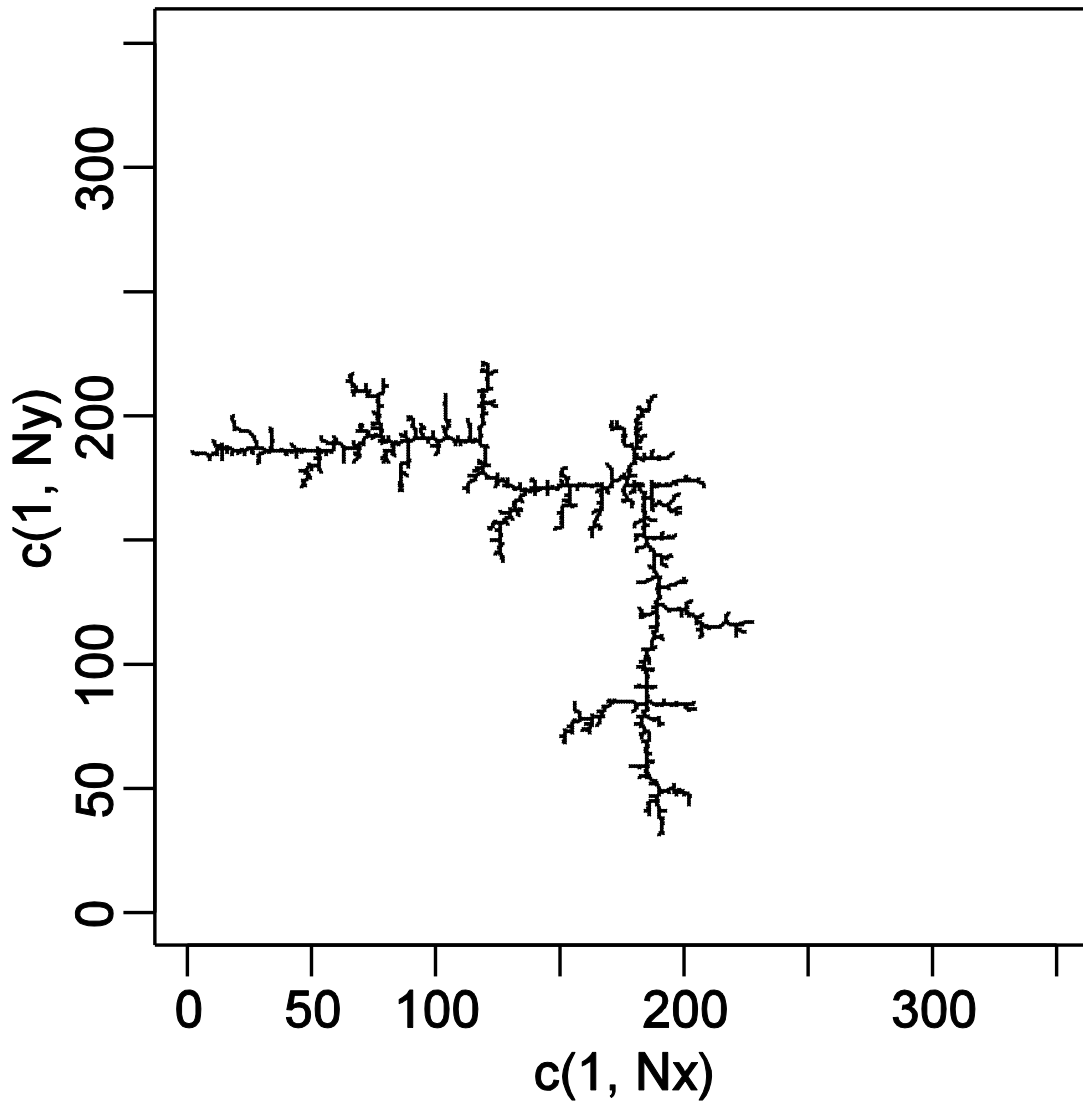


Figure 10. 1985 points plotted where the growth parameter $\eta=2$. A more spindly pattern emerges.

The length of branches or the number of points is cumulatively distributed according to

$$N(r) = A \left(\frac{r}{L} \right)^D$$

Where: N = number of points inside a given radius r
 A = some constant close to unity.

L = independent length scale

In a statistical analysis take the log of both sides of the above equation

$$\ln(N(r)) = \ln(C) + D \ln r, \text{ where } C \text{ is some constant.}$$

We notice quite a linear slope when we graph the regions between 20% and 60%. We shall choose this region to avoid end effects and where the slope is most linear. We do a least square fit between these points to determine the coefficient D .

First we see that our assumptions of fractal statistics is valid. Results: The results are shown below in figure 11 using a 5000 point model. There is excellent agreement with the published-simulation numbers for Hausdorff dimension. Recall the Hausdorff dimension controls the number of points inside a circle of radius r , where the exponent is not necessarily an integer. In the literature the point for $n=2$ had no error bars. This point has been omitted in the plot.

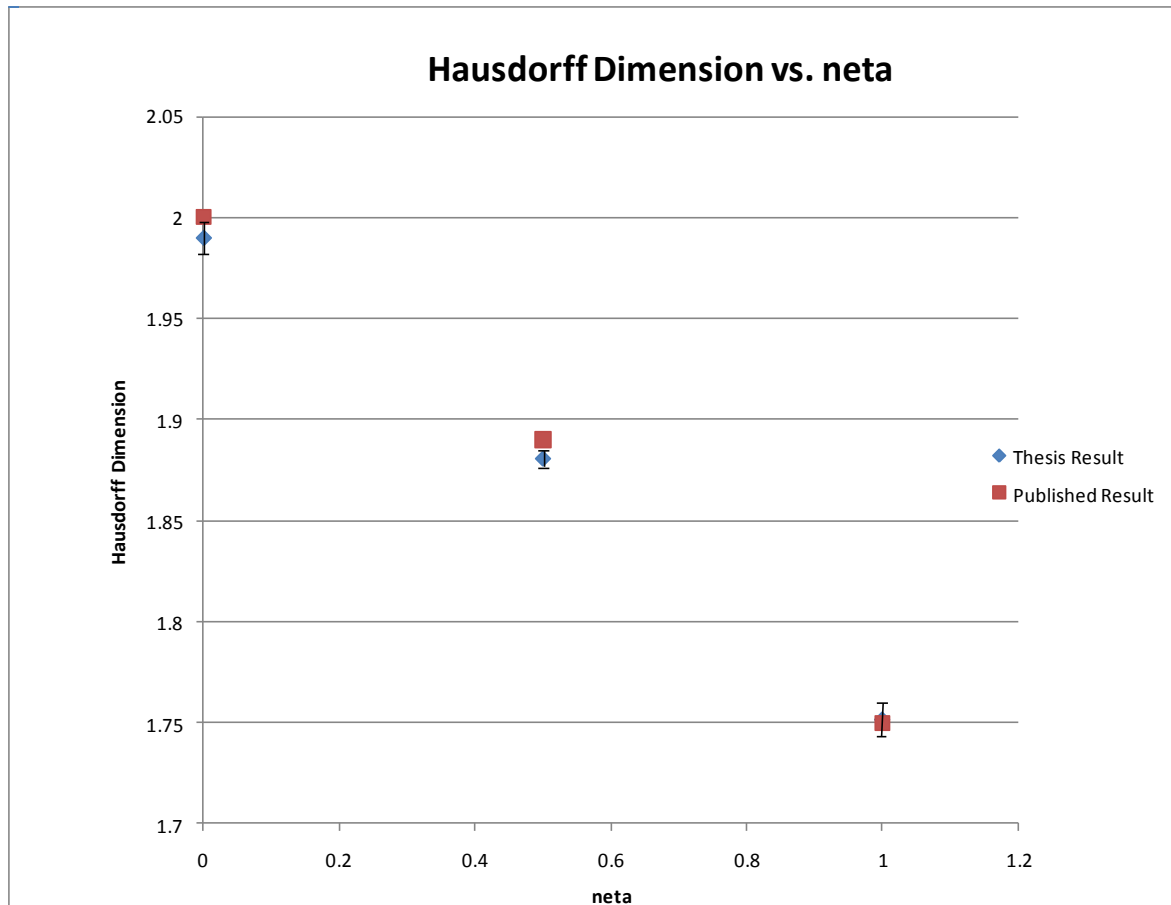


Figure 11. Hausdorff dimension vs. growth factor η .

4.2. Currents and fields

Next for the fractal pattern generated we will assume the following current $I(t)$ as per Valdivia et al. See figure 12 below.

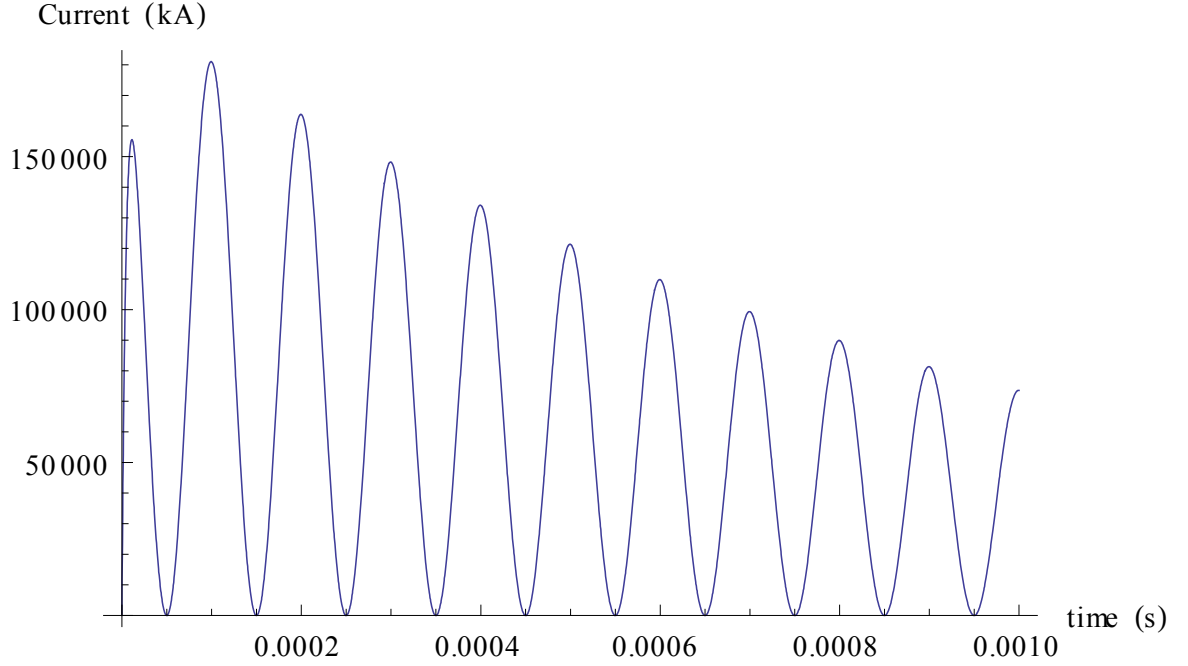


Figure 12. Current distribution assumed throughout the fractal.

$$I(t) = I_0 \left[e^{-\alpha t} - e^{-\gamma t} \right] (1 + \cos(\omega t) H(t)) \quad (2)$$

Where: $H(t)$ = Heavyside step function.

α =decay constant, $\alpha=10^3 \text{ s}^{-1}$.

γ =rise time, $\gamma=2 \times 10^5 \text{ s}^{-1}$.

$I_0=100 \text{ kA}$.

$\omega=2\pi\alpha n_f$

n_f =number of oscillations in the decay timescale $1/\alpha=10 \rightarrow 10 \text{ kHz}$.

The initial strength of the current pulse gets divided as the discharge branches. The total charge $Q \approx I_0/\alpha$, $I_0=100 \text{ kA}$, $Q=100 \text{ C}$. The damping constant α is constant with observations that show a time constant or decay of the order of a millisecond.

In the next couple of paragraphs we derive the fields for a fractal antenna. We then show the fields have the same dimension and form as Valdivia equations with a substitution for β the speed at which the discharge propagates along the fractal.

Consider a standard E&M radiation equation. Using the dispersed current throughout the branches of the fractal we get the far fields. From (Jackson 1975) the first term only, the electric field in the radiation zone is

$$\vec{E}_{rad} = \frac{\vec{P}_{\perp}''(t - r/c)}{c^2 r}. \quad (3) \text{ (Gaussian)}$$

The dipole moment P can be calculated by the following equation for sinusoidal variations (see Appendix 3)

$$-i\omega\vec{P} = \int d^3x \vec{J}(x).$$

Where: k = the free space wave vector

\vec{E}_{rad} = electric field in the radiation zone

c = speed of light

\vec{P}_{\perp} = perpendicular component of the electric dipole moment \vec{P}

$\vec{J}(x)$ = the current density on the wire

t = time

r = distance to the source

$t-r/c$ = the retarded time

$i = \sqrt{-1}$.

we have used : $k^2 = \frac{\omega^2}{c^2}$

$$\vec{n} \times \vec{p} \times \vec{n} = P_{\perp}$$

$$\omega^2 \Rightarrow -P_{\perp}''$$

\vec{n} = unit normal from the observation point to the source

Consider the current along a differential element in unit direction \hat{z} .

$$\vec{P} = \frac{idlI\hat{z}}{\omega}$$

Assume a basic dependence everywhere:

$$e^{i(kx - \omega t)}$$

$$\vec{P} = \vec{P}_0 e^{i(kx - \omega t)}, \text{ etc}$$

$$\vec{P}'' = -i\omega dl I \hat{z}$$

$$\vec{E}_{rad} = -\frac{i\omega dl I_0 (t - r/c)}{c^2 r} \hat{\theta} \quad (4) \text{ (Gaussian)}$$

The mks equivalent with a variation $e^{i(\omega t - kx)}$ is (Ramo and Winnery 1953)

$$\vec{E}_{rad} = \frac{\mu_0}{4\pi} \frac{i\omega dl I_0}{r} e^{-ikr} \hat{\theta} \quad (4) \text{ (mks)}$$

The sign is flipped because of his sign reversal in the wave equation dependence. Also in his equation a sine θ term has been evaluated at $\pi/2$ since the observation point is at right angles to the element of wire. The exponential dependence e^{ikr} is the same as saying the source is evaluated at the retarded time.

See Appendix 4 how to convert Gaussian to mks units.

From the equation for P with sinusoidal variation:

$$\vec{P}' = dl I \hat{z}$$

$$\vec{P}'' = dl \frac{dI}{dt} \hat{z}$$

$$\vec{E}_{rad} = \frac{dl \frac{dI(t - r/c)}{dt}}{c^2 r} \hat{\theta} \quad (5) \text{ (Gaussian)}$$

Valdivia's [3] far-field equation for the electric field is

$$\vec{E}(x, t) = \sum_n \frac{(\beta I_n I(\tau))_{t-\tau_2}^{t-\tau_1} \hat{L}_n}{cd_n (1 - \beta(\vec{L}_n \cdot \vec{d}_n))} \quad (6) \text{ (Gaussian)}$$

Where: I_n =fraction of current in branch

$I(\tau)$ =Eq. 2

$$d_n = |\vec{x} - \vec{r}_n|$$

$$\hat{d}_n = (\vec{x}_n - \vec{r}_n) / |\vec{x}_n - \vec{r}_n|$$

\vec{x} =observation point

\vec{r}_n = vector to the nth element

\hat{L}_n = orientation of the nth element

c =speed of light

$$\beta = \frac{v}{c} \approx .025$$

s_n = path along the nth element of fractal

$$\tau_1 = \frac{d_n}{c} + \frac{s_n}{v}$$

$$\tau_2 = \frac{d_n + (\hat{L} \cdot \hat{d}_n)L_n}{c} + \frac{s_n + L_n}{v}.$$

The following is not a proof but we can show in the limit of small β Valdivia's equation for the envelope waveform has the same form and dimension as is what was previously derived for our sinusoidal waveform.

$$\bar{E}(x, t) = \sum_n \frac{(\beta I_n I(\tau)) \Big|_{t-\tau_2}^{t-\tau_1} \hat{L}_n}{c d_n (1 - \beta(\bar{L}_n \cdot \bar{d}_n))}$$

$$\text{For } \beta = \frac{v}{c}$$

$$\bar{E}(x, t) = \sum_n v \frac{I(t - \tau_1) - I(t - \tau_2) \hat{L}_n}{c^2 d_n (1 - \beta(\bar{L}_n \cdot \bar{d}_n))}.$$

$$\text{For } v = \frac{dl}{dt} \text{ and } L_n \text{ along unit vector in the z direction}$$

$$\bar{E}(x, t) = \sum_n \frac{dl \frac{I(t - \tau_1) - I(t - \tau_2)}{dt} \hat{z}}{c^2 d_n (1 - \beta(\bar{L}_n \cdot \bar{d}_n))}.$$

$$\bar{E}(x, t) = \sum_n \frac{dl \frac{dI(t - r/c)}{dt} \hat{z}}{c^2 d_n (1 - \beta(\bar{L}_n \cdot \bar{d}_n))}$$

(7) (Gaussian)

For the derivative evaluated at a point instead of two limits and for small β this is the same form as Eq (5).

Once fields are calculated one could place them into the Folker-Plank equation or an ionization equation to see the effect of spider lightning on communications.

Now that we have the fields in terms of currents, the next step is to weight the branch currents. We expect the largest current to flow the longest in terms of time and path distance. This can be qualitatively seen in figure 1 where the strongest line patterns of discharge propagate the longest distance on the glass

plate. Weight the branch currents with length as in the figure 13 below. The current leaving each branch is assumed proportional to the path lengths.

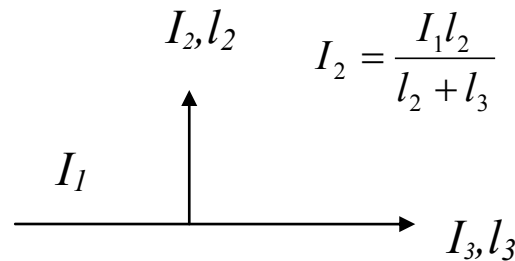


Figure 13. Weighting fractal branches with path length.

We have implemented the following algorithm to find the current flowing into that node. Keep the longest branch length and trace the length back one node before. Repeat this process until the origin is reached. We give an example. Say the path length of a top branch is six units and the path length of a bottom branch is four units. Keeping the longest path length (six units) we trace back five more units until we hit another branch point where a branch of length 10 units merges in. The sum of the branch lengths at the second junction is 21 units. Then the current flowing into the first top branch of the second junction would be $(11/21)$ of whatever flows into the second junction. Similarly the current flowing into the top branch of the first node would be the product of $(11/21)$ $(2/3)$ times any other factors for the accumulated current flowing into the second branch.

While this is quite easily stated it took a lot of time and effort to implement into the computer code. See figure 14 below for the block diagram of code. A sample output is found in Appendix 5. A complete description of the code is found in Appendix 6.

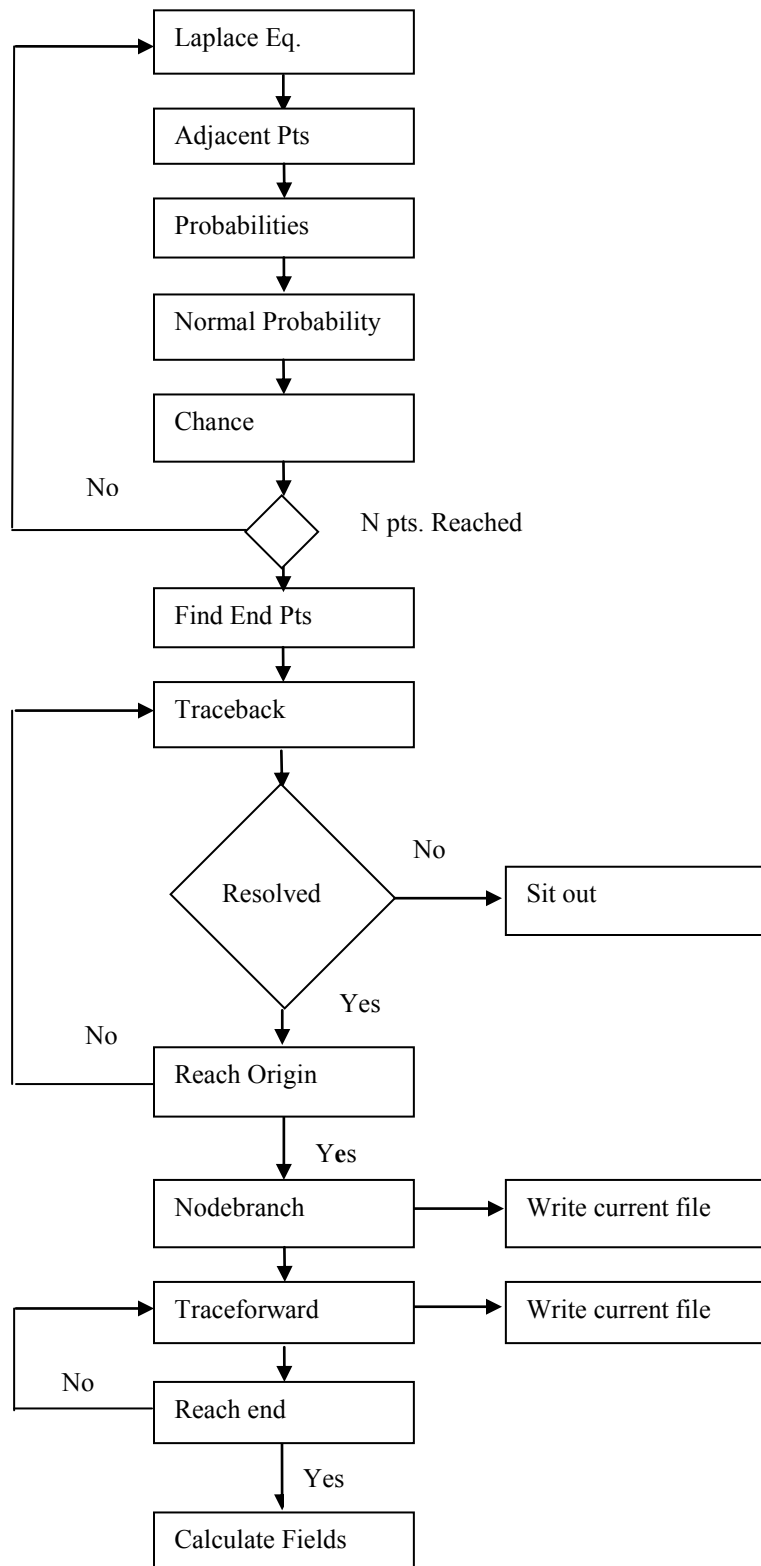


Figure 14. Flow chart of code.

5. Sample Output

Sample output is listed in Appendix 4. The current is written to a non orthogonal coordinate system. Hence if the current goes from point i, j to $i+1, j$, the current is listed at point $i+1/2, j$. The fraction of current is listed next to each point for currents in that branch. It has a unique index for later constructing electric fields. Also listed is the path length along the fractal to that element, and the orientation of the element along x or y axis.

After the coordinates and currents the start and stop points of the vectors are listed again with the currents and path length.

6. Plotted Output

The fraction of current in the output was checked by hand for eight cases of 10 points, and then three cases of 25 points. From here on we rely upon graphically checking the fractal pattern. In the following three patterns, figs. 15-17, the line weight represents the fraction of current in each branch. It can be seen that the black lines are like arteries carrying the current out to smaller sub-sections of the fractal. Each plot has 1000 points.

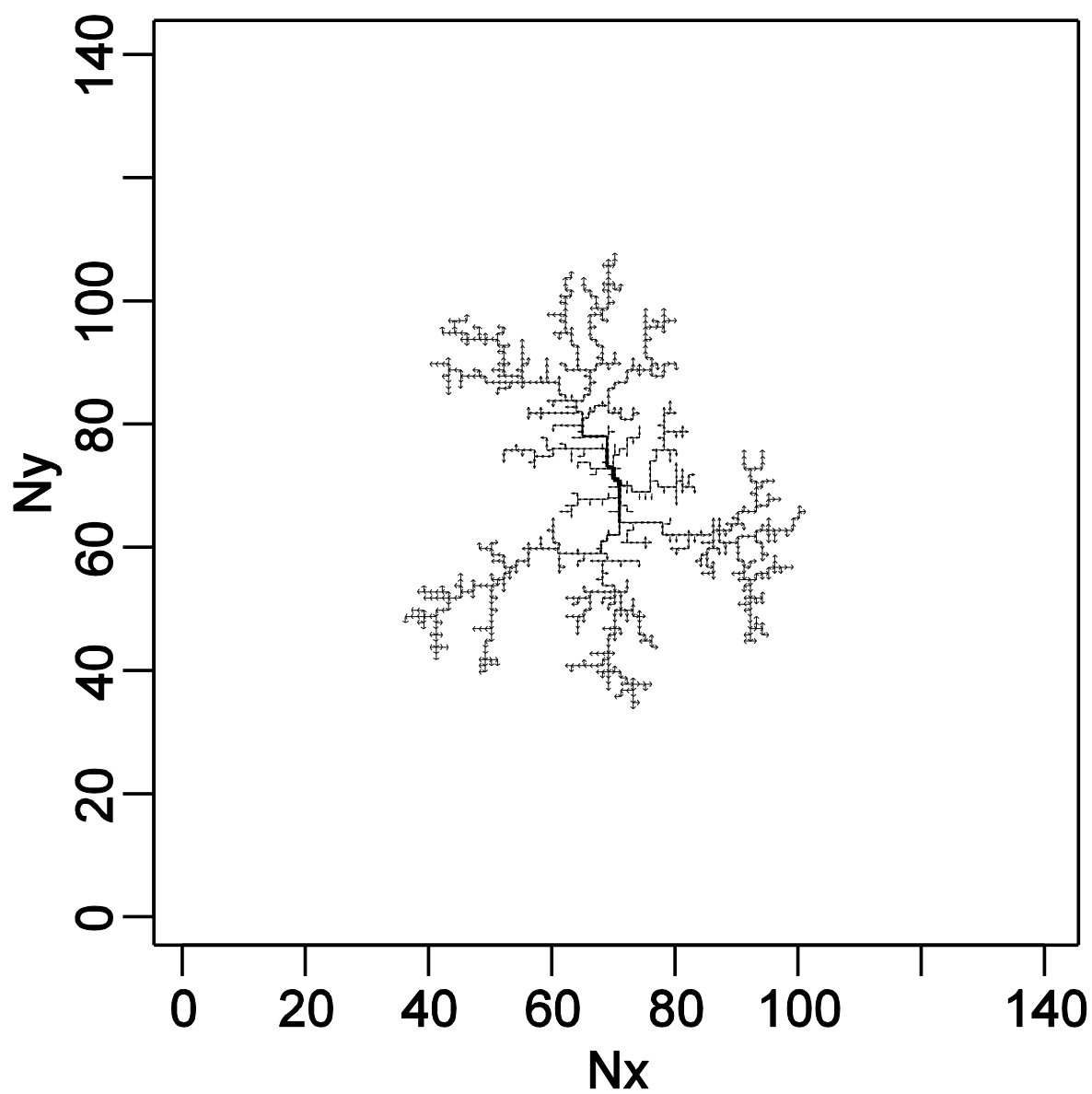


Figure 15. Fractal 1, 1000 points. Graphical validation of current weighted with path length.

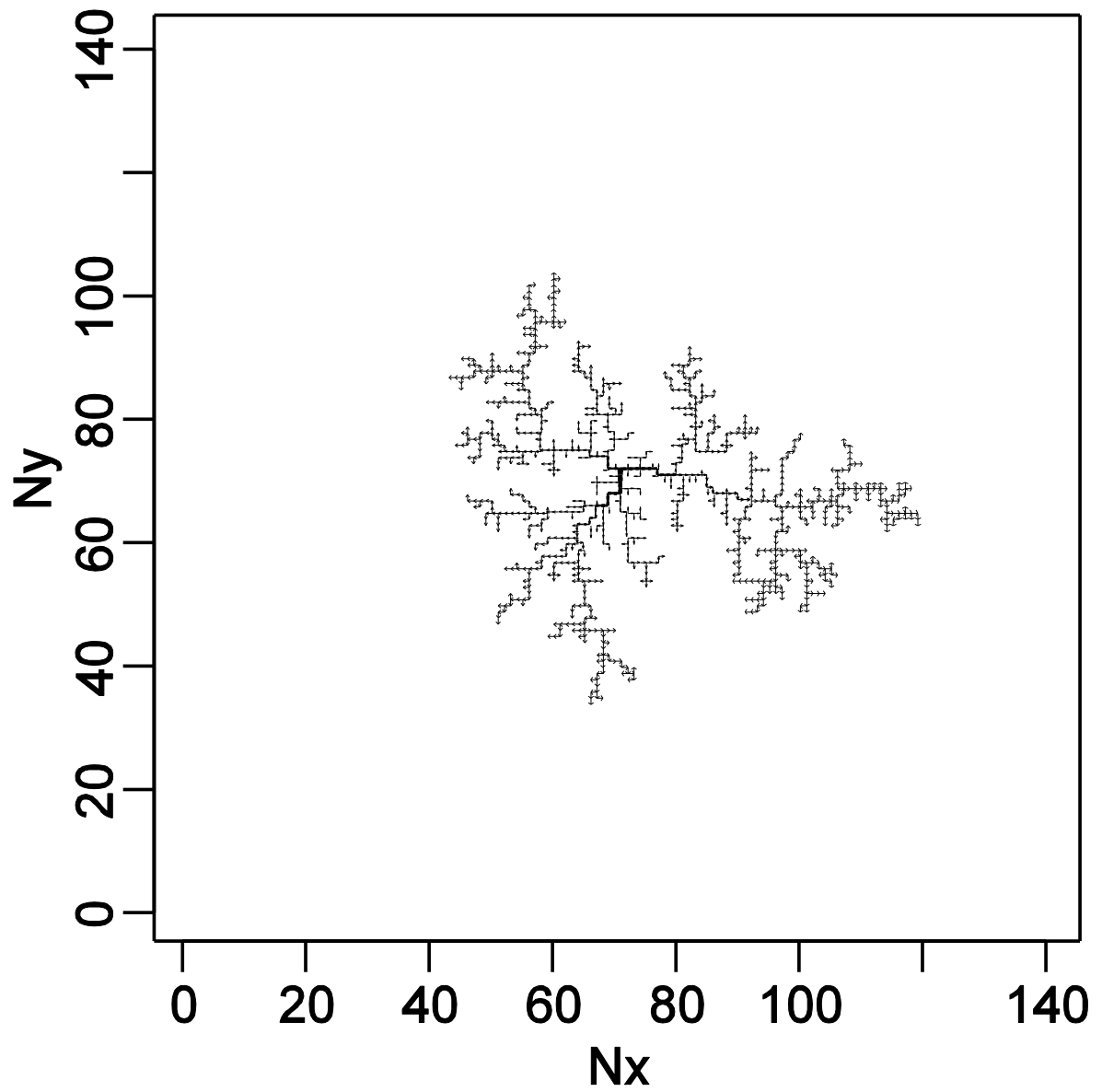


Figure 16. Fractal 2, 1000 points. Graphical validation of current weighted with path length.

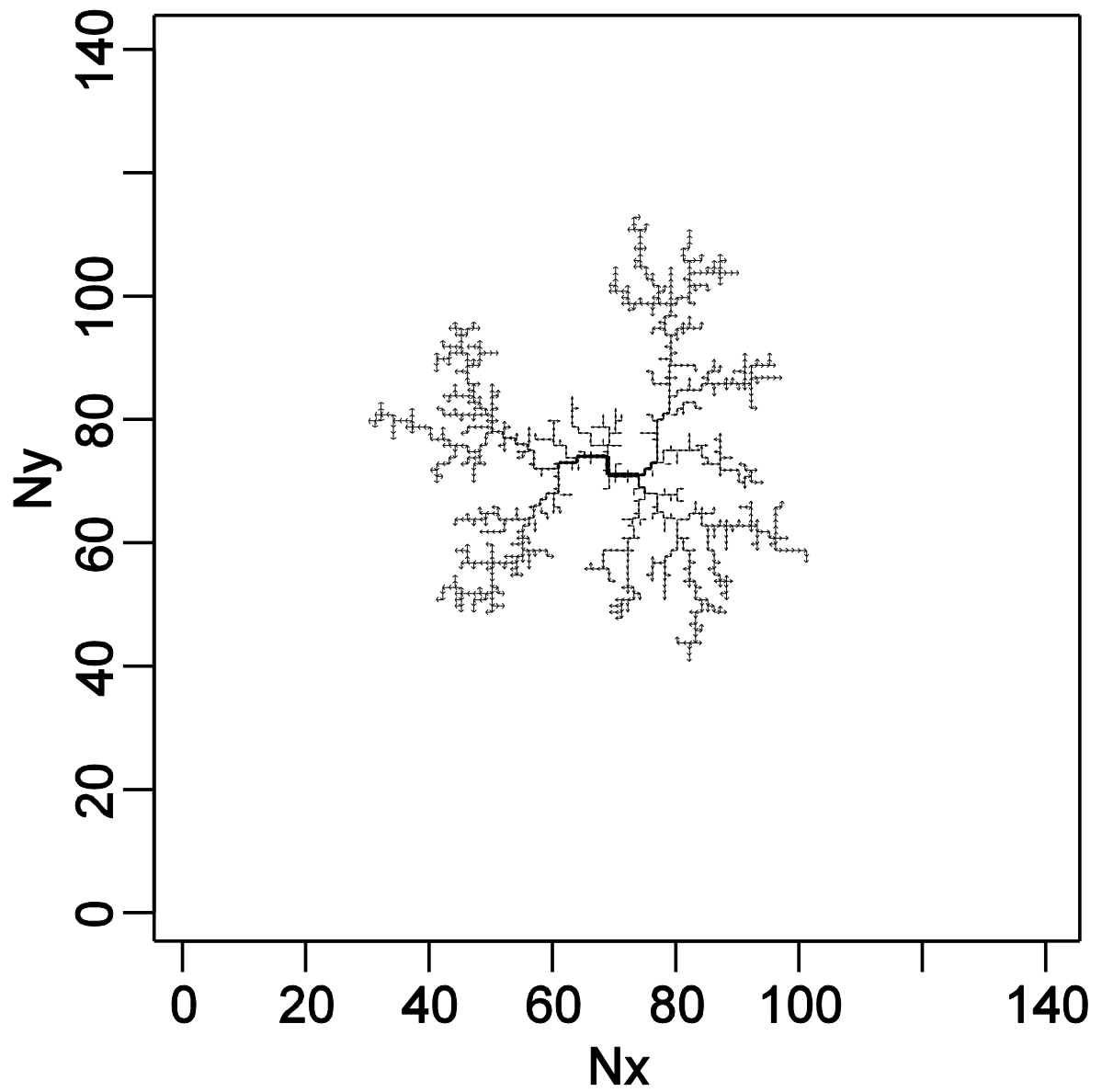


Figure 17. Fractal 3, 1000 points. Graphical validation of current weighted with path length.

7. Radiated Fields

Valdivia does not analyze the behavior of the radiated fields. In this section we calculate the fields from the fractal antenna, and show that the radiative fields obey a power law decay with increasing frequency.

7.1. Gain of Fractal Antenna

Valdivia (Valdivia et al. 1998) states the gain of a fractal antenna as

$$\vec{E} \cdot \vec{E}^* \approx \left(\sum_{n=1}^{\infty} A_n e^{in\varphi} \right) \cdot \left(\sum_{m=1}^{\infty} A_m e^{im\varphi} \right)^*$$

Where A_n = strength and orientation of the field generated by individual elements.

$$E \cdot E^* \approx G = N^2 \left(\frac{1}{N} + \frac{N-1}{N} |\langle e^{i\phi} \rangle|^2 \right)$$

If the distribution of phase is random $\langle e^{i\phi} \rangle = 0$, $G=N$. If the phase is perfectly coherent $G=N^2$.

7.2. Vecchi's Time Constant for Channel Lightning.

Let L be the scale length of the model, and v the velocity of propagation. The time constant τ is defined as $\tau = \frac{L}{v}$. For $freq < \frac{1}{2\tau}$ the power spectrum $\propto \frac{1}{f^2}$,

and the channel behaviors as a tortuous channel. For $freq > \frac{1}{2\tau}$ the power

spectrum $\propto \frac{1}{f^4}$, and the channel behaves as a straight line. This is because

high frequencies correspond to short evaluation times and in Vecchi's formulation certain terms can be ignored in the field evaluation. In general he says it obeys a

simple power law and decays as $\frac{1}{f^\beta}$. The spectral exponent β is found to vary

from $\beta = 4$ for a Euclidian curve ($D=1$) to a space filling curve ($D=2$). This dependence can be explained with the increase in high frequency components generated by increased irregularity of the evaluation times for large values of the fractal dimension D . This reduced the slope of the power spectrum.

The same time constant also appears in the frequency domain. The time lag between successive arrivals is proportional to L , the scale length. For small L we expect the field time waveform to be smooth. For large L we expect to see some fractal characteristics in the radiated fields.

7.3. Methodology

Fields in the far zone are now calculated by Eq. 6. All the necessary quantities are listed under the equation. A step counter in the software measures the distance from the origin to the center point of a fractal element. In the formula a dot product appears

$$\hat{L}_n \cdot \hat{d}_n \text{ Where } \hat{L}_n$$

is the unit vector orientation of the n^{th} element and \hat{d}_n is the unit vector

$$\hat{d}_n = \frac{(\vec{x}_n - \vec{r}_n)}{|\vec{x} - \vec{r}_n|} . \text{ The calculation proceeds as follows. The quantity}$$

$$\hat{r} = x\hat{i} + y\hat{j}, \hat{r} = \frac{\langle x, y \rangle}{\sqrt{x^2 + y^2}} . \text{ The observation point } \hat{x} = z\hat{z} . \text{ The quantity}$$

$$\hat{d}_n = \frac{(\vec{x}_n - \vec{r}_n)}{|\vec{x} - \vec{r}_n|} = \frac{\langle -x, -y, z \rangle}{\sqrt{x^2 + y^2 + z^2}} . \hat{L}_n \text{ has the orientation either along the x or y}$$

direction. Then the dot product $\hat{L}_n \cdot \hat{d}_n = \frac{-x}{\sqrt{r^2 + z^2}}$ if L_n is along the positive x

axis and $\frac{-y}{\sqrt{r^2 + z^2}}$ if L_n is along the positive y axis.

7.4. Results

Each element of the fractal is treated as a radiating segment, but the times that the overall current distribution are evaluated are delayed by the speed at which the lightning propagates along the fractal $\beta=0.025$. The propagation speed during a cloud-to-cloud return stroke can reach speeds of about $\beta \approx 0.1$ to 0.5 (Uman 1987), while the propagating speed of inter-cloud discharges is at least an order of magnitude lower, $\beta=0.01-0.05$. The number chosen is mid-range in

value. First a 10-element fractal was generated and the fields examined 90 km away. The field strength was similar to that of a single radiating element at full current. From this we gather that the individual elements were not acting coherently. This is due to their different orientation, and phasing.

Next the fields were calculated for a 1000 element fractal. As more elements are added or the scale increased the radiated field goes up. We also expect more interference between radiating elements. This is indeed the case. In figs. 18-20 the scale length of a fractal element is stepped from 1m, 10 m, and 100 m. In each case the same 'random' pattern used was that of figure 17, only the grid size changed. Notice that as the grid size increases the power in the signal increases as well as Fourier components above 10 KHz. This is displayed in either the vertical or horizontal polarization. Recall the source had a modulated component at 10 kHz. For a scale factor of 1 m the fractal antenna behaves as a normal antenna. Fourier components above 10 kHz fall off as some exponential. For scale factor of 10 m some fractal noise begins to appear above 10 kHz. For a scale factor of 100 m, figure 20, the radiated fields begin to exhibit some fractal characteristics. There is an initial spike in the vertical and horizontal field component for the typical case with scale lengths of 1 m. The fields go as the derivative of the currents, the currents turn on as a Heavy side step function, hence in taking the derivative of the current there is a delta function. The spike goes away in time and also is not present for scale lengths of 10 and 100 m. Observing the time domain waveform near the end the signal becomes smoother in time as the discharge travels to the end of the fractal.

We found areas of the FFT where the curve exhibited smooth or non-fractal behavior (1 & 10 m scale length above or near 10 kHz). Vecchi states for the fractal noise there is an *asymptotic region* (for large frequencies). We note for the frequency below this is an upper bound of only one region. Vecchi's threshold frequency with scale=100 m and $\beta=0.025$ yields $\tau=1.33 \cdot 10^{-6}$ s or $f_{\text{threshold}} = 37.5$ kHz. For *channel lightning* and frequencies less than this threshold frequency the radiated power falls off approximately 20 dB/decade if the power goes as one over the frequency squared (see proof below).

Proof that if power $\propto 1/f^2$ the power falls off at -20 dB per decade

$$P = \frac{c}{f^2}$$

$$\frac{P_2}{P_1} = \left(\frac{f_1}{f_2} \right)^2$$

$$10 \log \left(\frac{P_2}{P_1} \right) = 20 \log \left(\frac{f_1}{f_2} \right)$$

Aside:

$$f_1 = \frac{1}{10} f_2 \text{ per decade}$$

Then the left hand side is power in dBs, on the right hand side $\log(f_1/f_2) = -1$, therefore

$$P_2(\text{dB}) = -20\text{dB} / \text{decade}$$

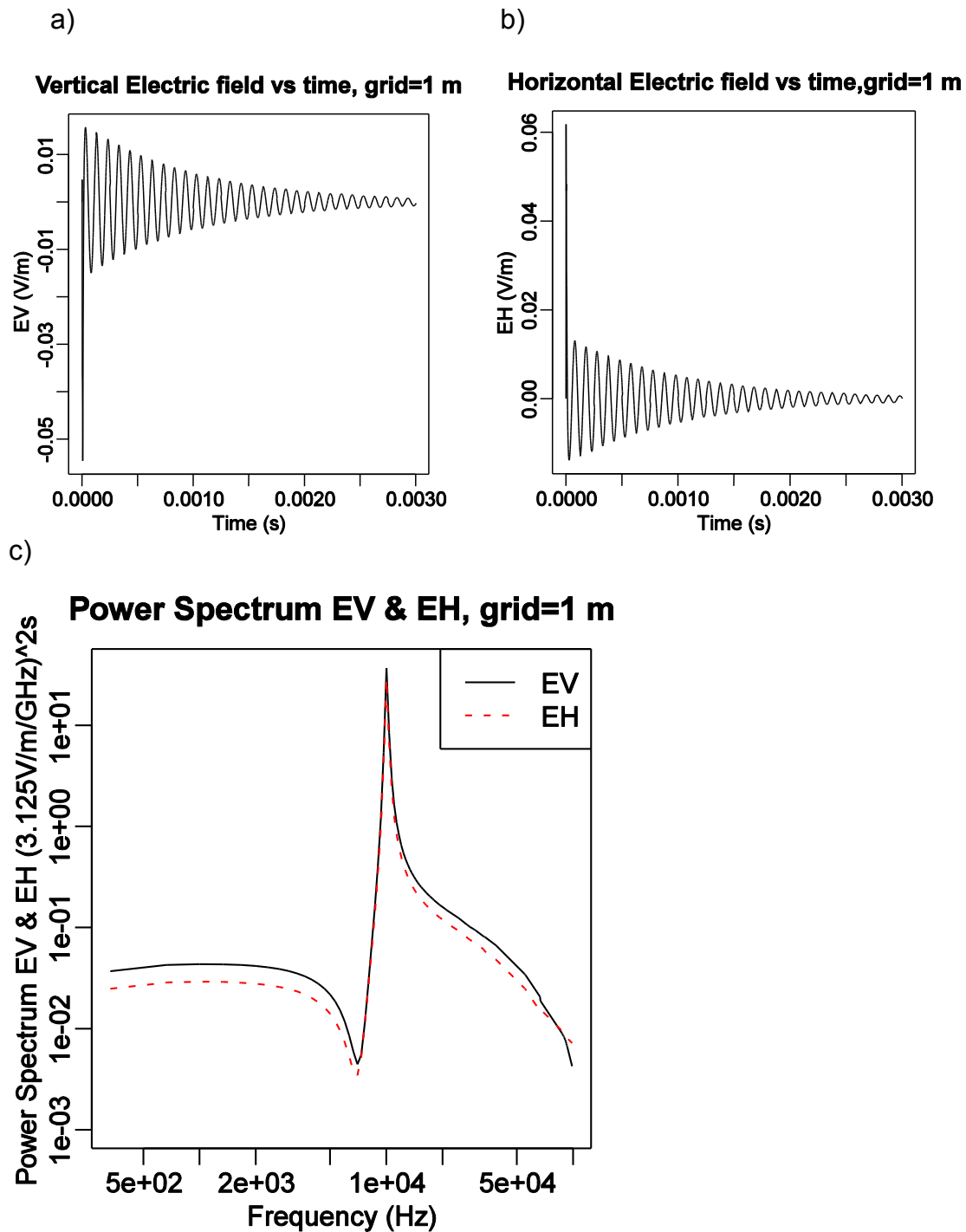


Figure 18. Magnitude of electric field, vertical and horizontal components, with Fourier transform. At grid = 1 m it acts just as an antenna where frequencies taper off smoothly above 10 kHz.

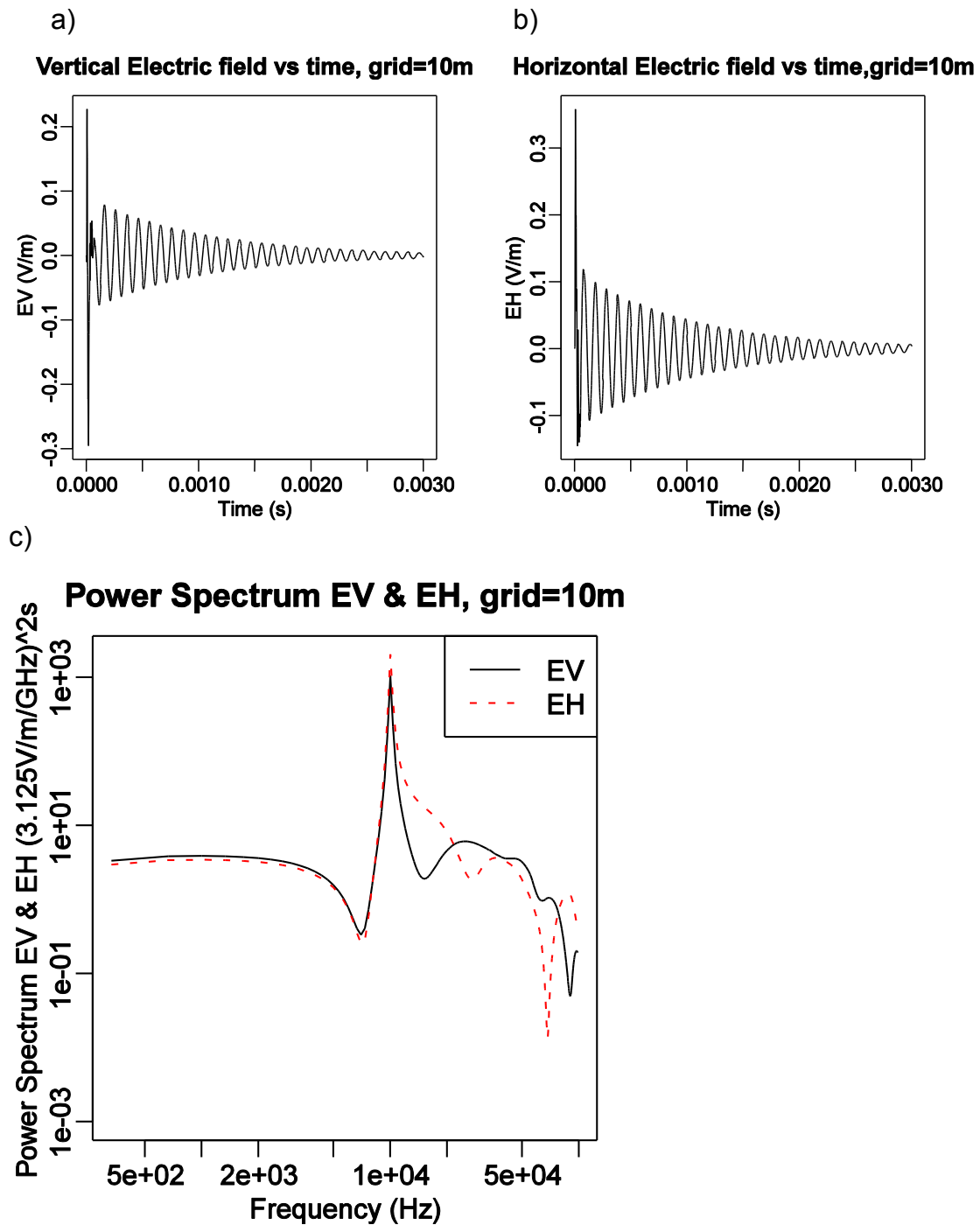


Figure 19. Magnitude of electric field, vertical and horizontal components, with Fourier transform. At grid = 10 m some fractal noise begins to appear above 10 kHz.

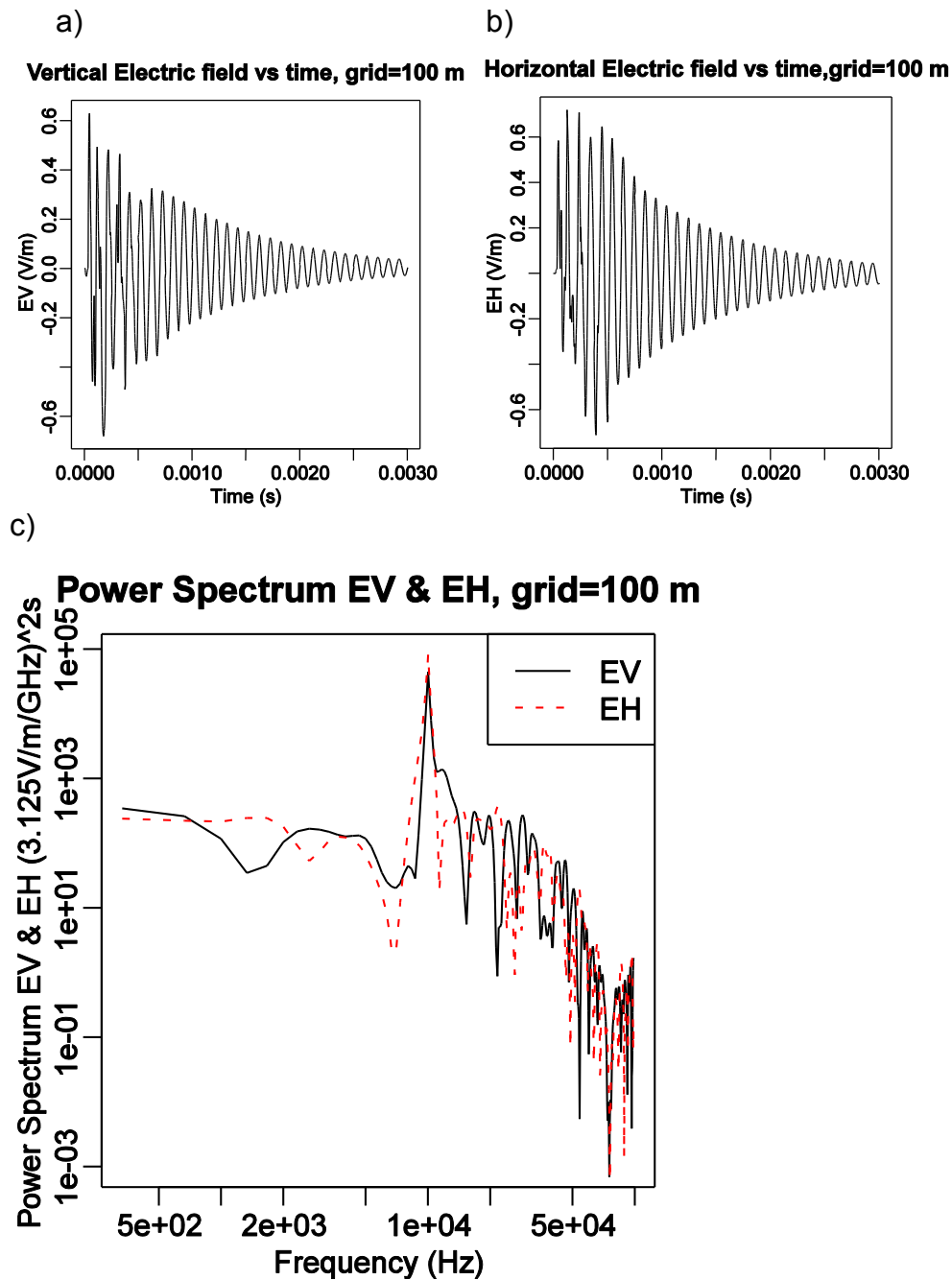


Figure 20. Magnitude of electric field, vertical and horizontal components, with Fourier transform. At grid = 100 m substantial fractal noise becomes apparent above 10 kHz.

8. Slope of the Power Spectrum

In this section we present slopes of the power spectrum for a grid scale of 100 m. We examine the noise in the spectrum above $1.67 * 10$ kHz. We purposely stay away from 10 kHz because this is the modulation frequency imposed upon the current. This region is divided into two regimes. One regime is $f < f_{\text{threshold}}$ and another is $f > f_{\text{threshold}}$. Vecchi's threshold frequency is

$$f_{\text{threshold}} = \frac{1}{2\tau} \text{ where } \tau \text{ is the time to cross a fractal element. Quantity } \tau = \frac{100m}{\beta c}$$

where $\beta=0.025$, and c is the speed of light. The graphs presented in the next two figures are typical but the author found quite a lot of variation in the slope $f < f_{\text{threshold}}$, even among case to case, with the same η . The plotting program had some difficulty plotting the right set of points in the log format, but could plot them without error on a linear plot. We use a least square fit to eliminate subjectivity. The slopes are averaged over 50 runs each and presented below. Quantity EV is the vertical- electric-far-field component and EH is the horizontal-electric-far-field component.

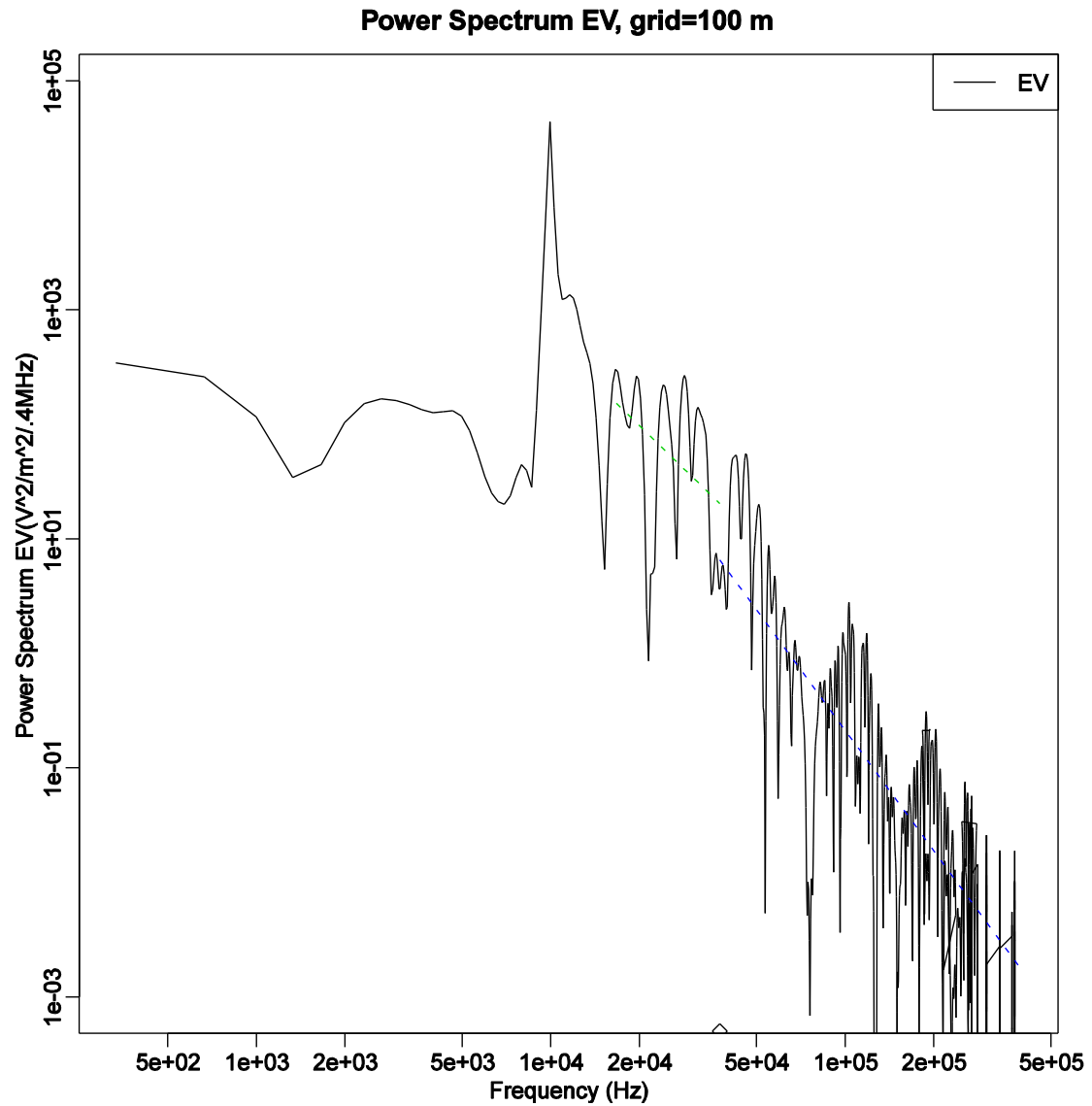


Figure 21. Slope of the EV power spectrum $f < f_{\text{threshold}}$ slope=2.5 and $f > f_{\text{threshold}}$ slope=3.5 . Triangle at bottom abscissa is where $f_{\text{threshold}}$ is.

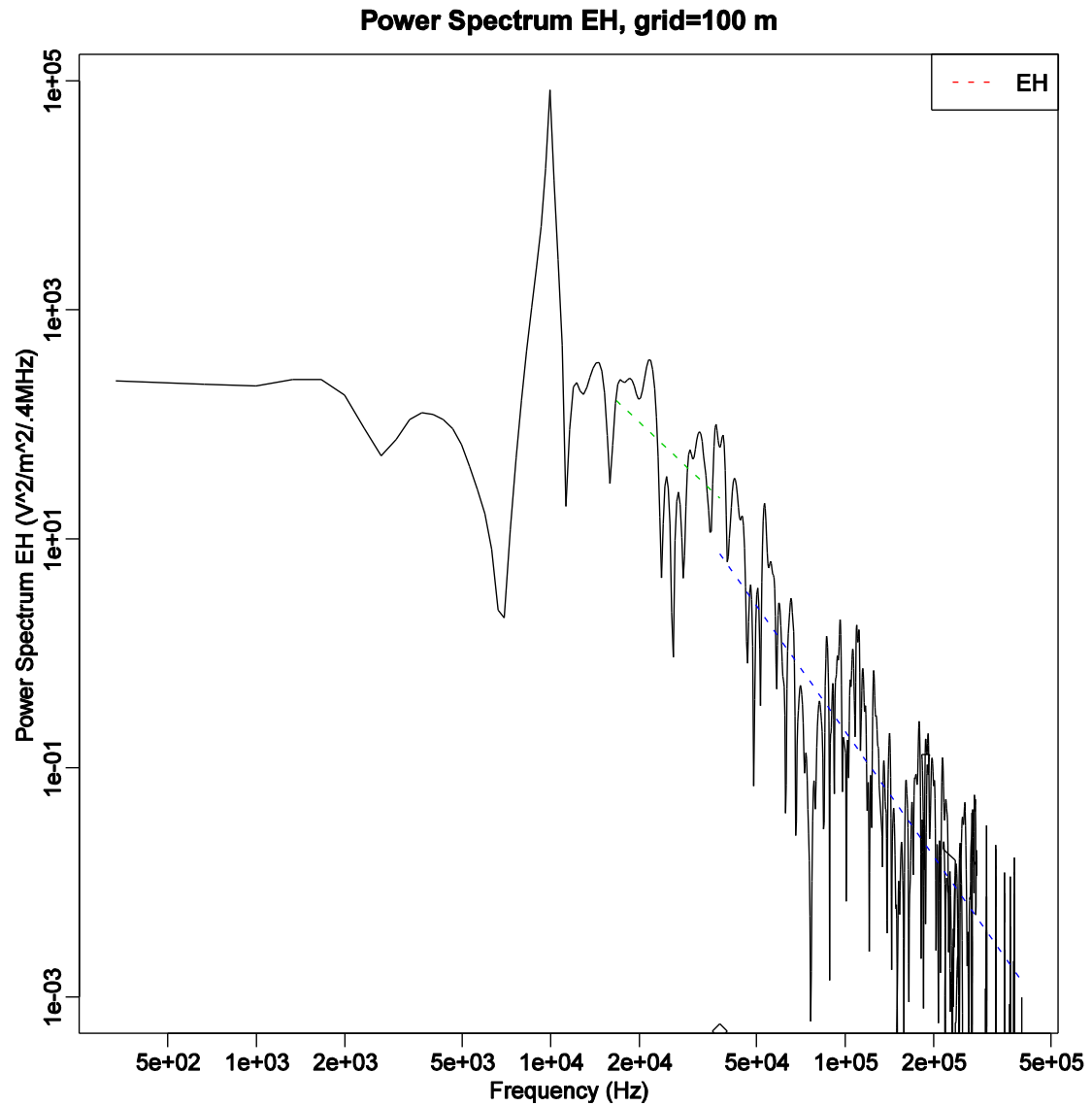


Figure 22. Slope of the EH power spectrum $f < f_{\text{threshold}}$ slope=2.4 and $f > f_{\text{threshold}}$ slope =3.6 . Triangle at bottom abscissa is where $f_{\text{threshold}}$ is.

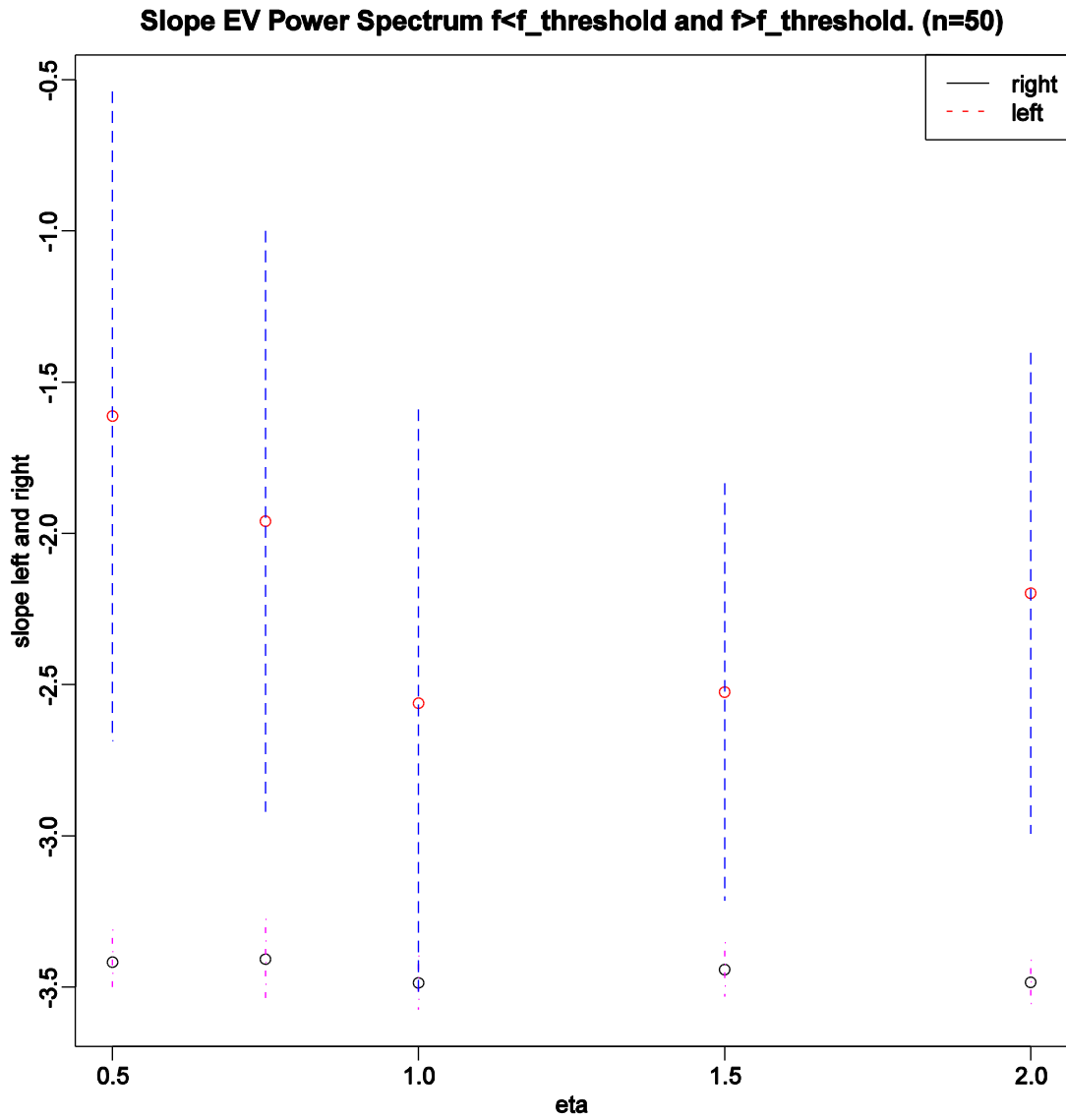


Figure 23. Average slope of EV $f < f_{\text{threshold}}$ and $f > f_{\text{threshold}}$ (n=50). Error bars denote standard deviation over 50 runs each.

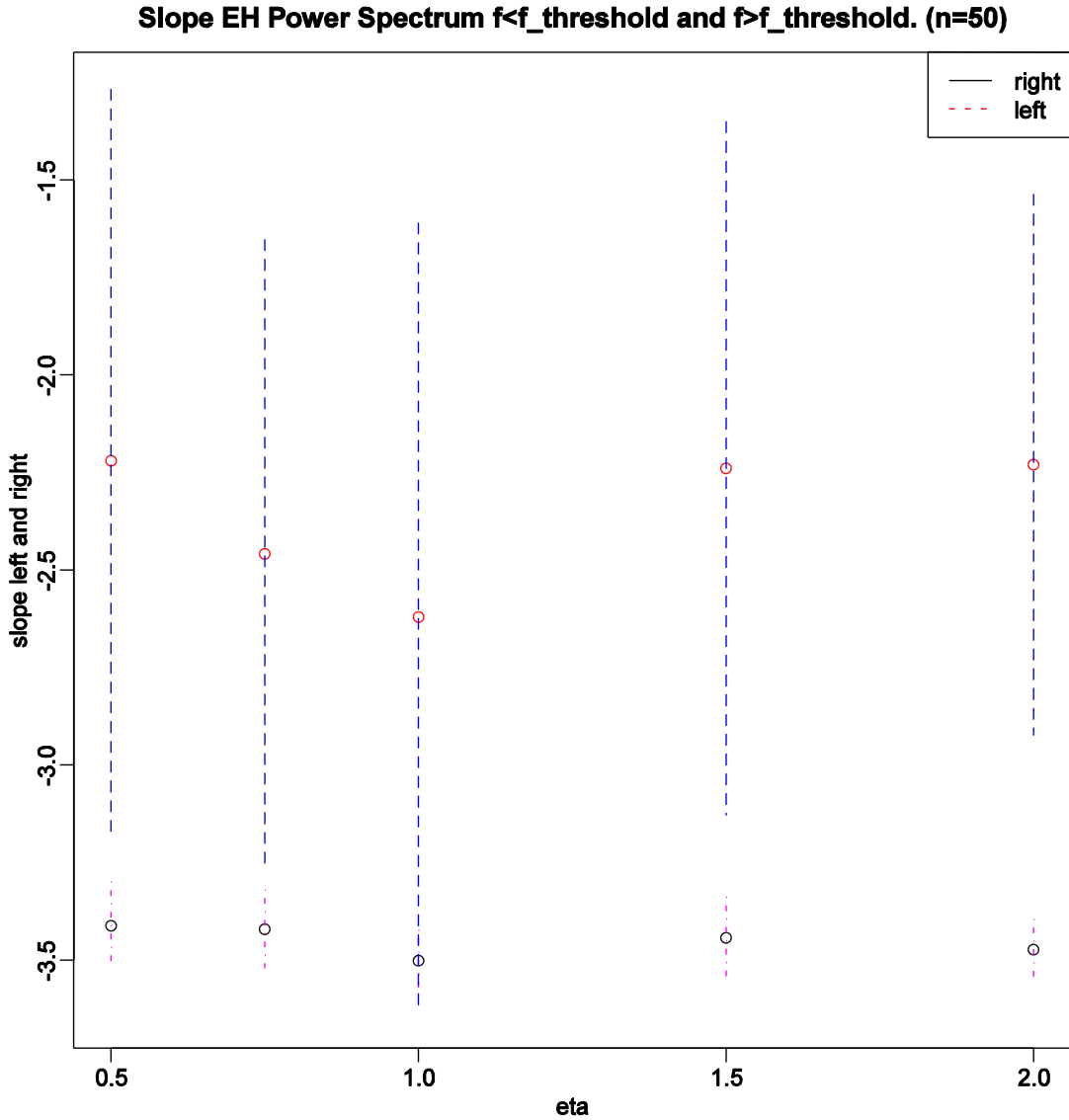


Figure 24. Average slope of EH $f < f_{\text{threshold}}$ and $f > f_{\text{threshold}}$ (n=50). Error bars denote standard deviation over 50 runs each.

Vecchi states for *channel lightning* the slope for $f < f_{\text{threshold}}$ should be -2. We observe an average slope in the range of -1.6 to -2.6 with a standard deviation of around 2. Again for *channel lightning* the slope for $f > f_{\text{threshold}}$ should be -4. We observe an average slope in the range of -3.4 to -3.5 with a standard deviation equal to or less than 0.25 for different values of η (Figure 23-24). Please refer to the individual graphs for standard deviations specific to a certain value of η . The

values are reasonable. Clearly this model is more complex than channel lightning for it has radial arms spreading in the x, y plane.

There doesn't seem to be much information for $f < f_{\text{threshold}}$. This data has quite a large standard deviation. However for $f > f_{\text{threshold}}$ the values appear to be independent of η . The values recorded here -3.4 to -3.5 are less than -4 for channel lightning because there is more interference between radiating elements in this fractal model than the case of channel lightning.

From observation, for vertical return strokes in the frequencies considered here, the power spectrum goes as $1/f^2$ (Shumpert, Honnell and Lott August 1982). For horizontal inter-cloud lightning (Marney and Shanmugam 1971) the noise spectrum is flat from 10 kHz to 50 kHz, and then dropped off with a slope of -1.6 for higher frequencies. This is because considerable energy comes from cloud-to cloud at higher frequencies. These events are harder to correlate because they are obscured by clouds. In the spider lightning model the slopes need roughly a value of 2 subtracted from them to match experiment. The threshold frequency with a grid scale of 100 m seems to be correct, 37 kHz vs. 50 kHz.

9. Future Work

For $f < f_{\text{threshold}}$ the values exhibit quite a large standard deviation (~ 2). The error of the mean, $\text{Error} \propto \frac{\sigma}{\sqrt{n}}$, where σ is the standard deviation. In order to get the error down to 0.1 from a standard deviation of 2 one would have to sample 400 cases each. One could set up a large sequence of runs on a pair of dual processor computers and check the results a month later to better find the functional dependence of this slope on η .

10. Conclusion

A program has been developed that performs the fractal modeling of lightning, and then calculates the radiated fields for this fractal antenna. The branch currents are proportional to the length of branch from the node in

question. Current into that node is calculated by taking the longest branch and tracing back one node before...and so forth, all the way until the origin is reached. For different growth parameter η the Hausdorff dimension agrees with those in the literature. Finally electric fields in the far zone have been calculated by weighting the branch currents with an overall damped sinusoidal current. The current waveform for each element is evaluated at retarded times and this also takes into account the speed at which the lightning propagates along the fractal. The electric field seems to be proportional to the number of elements, which means the elements are operating incoherently. With increasing grid size an interference pattern becomes more evident. As the grid size increases the power in the signal increases in the Fourier components above 10 kHz (the modulation frequency), in both polarizations. Finally for a scale factor of 100 m, the signal exhibits some fractal characteristics. We have investigated the slope of the power spectrum for spider lightning. For $f < f_{\text{threshold}}$ the slope is between -1.6 to -2.6 with a standard deviation of ~ 2 . In the case of channel lightning this slope would be -2. For $f > f_{\text{threshold}}$ the average slope varies between -3.4 and -3.5. In the case of channel lightning this slope would be -4. The lesser slope is attributed to more interference between radiating elements in this model. For $f > f_{\text{threshold}}$ the slope appears to be independent of the growth parameter η . Observations show for inter-cloud lightning the threshold frequency is 50 kHz, with zero slope for $f < f_{\text{Thresold}}$ and -1.6 slope for $f > f_{\text{Thresold}}$. The slopes for this model of spider lightning needs roughly 2 subtracted from them to match experimental results.

Appendix 1
Folker-Plank Equation.

$$\frac{\partial f}{\partial t} - \frac{1}{3mv^2} \frac{\partial}{\partial v} \left[v^2 \nu(v) \tilde{\varepsilon}(E, \nu(v)) \frac{\partial f}{\partial v} \right] = L(f)$$

Where:

$$\tilde{\varepsilon}(E, \nu) = \frac{e^2 E_0^2}{m[\Omega_B^2 + \nu^2]} \left[1 + \left(\frac{\Omega_B}{\nu} \right)^2 \cos(\theta_0)^2 \right]$$

$\tilde{\varepsilon}(E, \nu)$ is the quiver energy KE of electron oscillating field

$\nu(v)$ is the electron neutral effective collision frequency

L is the operator which describes the effect of inelastic collisions

θ_0 is the angle between the electric and magnetic field

ν = velocity of electron

Appendix 2

Code Sample Used to Solve the Laplacian.

The program R works with objects.

```

xp<-seq(-Nx/2,Nx/2,length=Nx)
yp<-seq(-Ny/2,Ny/2,length=Nx)
xmat <- xp%o%rep(1,Ny)
ymat <- rep(1,Nx)%o%yp
radmat <- sqrt(xmat^2+ymat^2)
hit <- radmat<=.5 Nx
radp1 <- sqrt((xmat-1)^2 + ymat^2)
hitxp1 <- radp1<=.5 Nx
radm1 <- sqrt((xmat+1)^2 + ymat^2)
hitxm1 <- radm1<=.5 Nx
radp1 <- sqrt(xmat^2+(ymat-1)^2)
hityp1 <- radp1<=.5 Nx
radm1 <- sqrt(xmat^2+(ymat+1)^2)
hitym1 <- radm1<=.5 Nx
laplace<-function(theta,val,fixed)
{
  for(iter in seq(1,itermax,1))
theta[hit] <- (theta[hitxp1]+theta[hitxm1]+theta[hityp1]+theta[hitym1])/4

  return(theta)
}

```

The boundary for the circle is described as follows. From a column vector of all x values along a line there is formed an outer product to get the x values of all points in a square array. A similar operation is done for y vertices along a line. Then the radius of all points from the origin in the square array computed. A logical matrix, hit, is computed where True values are assigned for all points less than a certain radius. To calculate $\phi(x + \Delta x)$ points the x values are shifted by

one grid point and a new logical matrix hitxp1 constructed. Similarly for $\phi(x - \Delta x)$ points and similarly shifted y values matrices are constructed which enter into the Laplacian. The field variable theta[hit] is solved for in a single line in the routine Laplace.

Appendix 3

$$\text{Identity } \int d^3x J = -i\omega \vec{P}$$

$$\text{Start From } \nabla \cdot (x_j J) = \nabla x_j \cdot \vec{J} + x_j \nabla \cdot \vec{J}$$

$$\nabla \cdot (x_j J) = J_j + x_j \nabla \cdot J \quad (1)$$

From the equation of continuity $\nabla \cdot J + \frac{\partial \rho}{\partial t} = 0$ and a basic dependence $e^{i(kx - \omega t)}$

quantity $\nabla \cdot J_j = i\omega \rho$ sub into (1)

$$\nabla \cdot (x_j J) = J_j + i\omega x_j \rho$$

$$\therefore J = e_j \nabla \cdot (x_j J) - i\omega \rho \vec{x}$$

$$\int d^3x J = e_j \int d^3x \nabla \cdot (x_j J) - i\omega \int d^3x \vec{x} \rho$$

$$\text{Applying the divergence theorem } \int d^3x \nabla \cdot (x_j J) = \oint_S x_j \vec{J} \cdot d\vec{a} = 0$$

The integral $\int d^3x \vec{x} \rho = \vec{P}$ the dipole moment, therefore

$$\int d^3x \vec{J} = -i\omega \vec{P}$$

Appendix 4

How to Convert Gaussian to mks

After (Jackson 1975):

$$J = \rho v$$

$$\frac{I}{A} = \rho v$$

where J is the current density and v the velocity and I the current. Along a thin wire: $I = \lambda v$, λ charge per unit length.

Making the proper mks substitutions for charge density and velocity. Symbols for time and length remain unchanged.

$$I_{guuss} = \frac{1}{\sqrt{4\pi\epsilon_0}} \lambda_{mks} v_{cgs}$$

$$I_{guuss} = \frac{1}{\sqrt{4\pi\epsilon_0}} \lambda_{mks} v_{mks}$$

Into Eq. 4 Gaussian $\frac{1}{c^2} \Rightarrow \mu_0 \epsilon_0$

$$E_{mks} \sqrt{4\pi\epsilon_0} = \frac{dl i \omega I_{0mks} \mu_0 \epsilon_0}{r_{mks} \sqrt{4\pi\epsilon_0}}$$

$$E_{mks} = \frac{\mu_0}{4\pi} \frac{dl i \omega I_0}{r} \quad (\text{sinusoidal variation}) \quad (4 \text{ mks})$$

Which is equation 4, mks, where we have dropped the mks subscripts from the right hand side

Appendix 5

Sample Output

```

igrid[[ 1 ]][[1]]= 21 21.5 fraction of current= 0.625 path length= 1 orientation
(nx,ny)= 0 1
igrid[[ 2 ]][[1]]= 21.5 21 fraction of current= 0.125 path length= 1 orientation
(nx,ny)= 1 0
igrid[[ 3 ]][[1]]= 21 20.5 fraction of current= 0.25 path length= 1 orientation
(nx,ny)= 0 -1
igrid[[ 4 ]][[1]]= 20.5 20 fraction of current= 0.25 path length= 2 orientation
(nx,ny)= -1 0
igrid[[ 5 ]][[1]]= 21 22.5 fraction of current= 0.5 path length= 2 orientation (nx,ny)=
0 1
igrid[[ 6 ]][[1]]= 20.5 22 fraction of current= 0.125 path length= 2 orientation
(nx,ny)= -1 0
igrid[[ 7 ]][[1]]= 21 23.5 fraction of current= 0.125 path length= 3 orientation
(nx,ny)= 0 1
igrid[[ 8 ]][[1]]= 20.5 23 fraction of current= 0.375 path length= 3 orientation
(nx,ny)= -1 0
igrid[[ 9 ]][[1]]= 19.5 23 fraction of current= 0.375 path length= 4 orientation
(nx,ny)= -1 0
igrid[[ 10 ]][[1]]= 19 23.5 fraction of current= 0.375 path length= 5 orientation
(nx,ny)= 0

```

```

21 21 21 22 0.625 1
21 21 22 21 0.125 1
21 21 21 20 0.25 1
21 20 20 20 0.25 2
21 22 21 23 0.5 2
21 22 20 22 0.125 2
21 23 21 24 0.125 3
21 23 20 23 0.375 3
20 23 19 23 0.375 4
19 23 19 24 0.375 5

```

Appendix 6

How the Program Works and Summary of Subroutines

Laplace:

Solves Laplaces equation for all points $r \leq N_x/2$, where r is the radius of grid points to the center and N_x is the number of x points on a grid. For $r > N_x/2$ the potential ϕ is set equal to unity.

Adjacentpts:

This constructs a logical matrix (True, False) of neighbors.

Probabilities:

Computes the numerator of Eq. 1 for all neighbors.

Normalprob:

Computes the denominator of Eq. 1 for all neighbors.

Chance:

Picks a random number from 0 to 1. Probabilities of each point are weighted with $P \propto |E|^n$. Picks a new neighbor to be added to the structure of grounded points.

Find end points:

Catenates vectors in situ as they are added. A vector starts at the beginning point of the grounded structure and ends at an end point of a newly added neighbor. Chains vectors onto existing branches. If not starts a new branch. Last chained vector of a branch contains the end point. These are used in the subroutine Traceback to find the branch currents.

Map:

Lists the i, j neighbors of any point (not used). Lists the NESW logical variables for currents into a node, where N is the north point, etc. Lists the sum of logical variables into a node. Lists the NESW path lengths into a node. Contains a logical variable if the node is resolved. A node is resolved if the code can sum the path lengths into a node and the number of path lengths summed equals the number of currents into a node. If the node is not resolved it 'sits' out. Has a logical variable for an end point. Has logical variables NSEW for currents emanating from a node. Two or more of these constitute a node.

Traceback:

Given an i, j of an end point or node traces back the branch until it reaches another node or the center point. A node is defined if more than one current emanates from the branch. This routine sums the branch length. Labels each branch sequentially by the assigned number of end points.

Resolved:

A node is resolved if the code can sum the paths of branches into a node and the number of paths summed equals the number of currents emanating from the node. Labels resolved nodes sequentially.

Nodebranch:

Determines the branches emanating from a node. A counter steps one grid point for each direction stepped. Calls subroutine Traceforward. Writes a current to a non-orthogonal grid. Current file has a unique index for a current written at every path.

How the Program Works

Every time Traceback is called the program collects resolved nodes. Labels them sequentially, level=1, resolved nodes =1-3. Node(1) = l_1, j_1 , node(2)= i_2, j_2 , node(3)= i_3, j_3 . Level =2, node(4)= i_4, j_4 , node(5)= i_5, j_5 . When no new nodes are accumulated it has reached the origin. Then it runs through the level of nodes in reverse order. Each node in the sequence is traced forward. Subroutine Nodebranch call trace subroutine Forward. Both write current files. They stop when another node or end point is reached.

References

- Bell, T. F., V. P. Pasko & U. S. Inan (1995) RUNAWAY ELECTRONS AS A SOURCE OF RED-SPRITES IN THE MESOSPHERE. *Geophysical Research Letters*, 22, 2127-2130.
- Cheng, Z., S. A. Cummer, H. T. Su & R. R. Hsu (2007) Broadband very low frequency measurement of D region ionospheric perturbations caused by lightning electromagnetic pulses. *Journal of Geophysical Research-Space Physics*, 112.
- Gou, X. Q., M. L. Chen, Y. J. Zhang, W. S. Dong & X. S. Qie (2009) Wavelet multiresolution based multifractal analysis of electric fields by lightning return strokes. *Atmospheric Research*, 91, 410-415.
- Gurevich, I. S. (1977) Changing Ionization of the lower Ionosphere due to High-Power Radio waves. *Radiofizika*, 20, 1790-1804.
- Jackson, J. D. 1975. *Classical Electrodynamics*. NYC: John Wiley & Sons.
- Kerr, R. A. (1994) ATMOSPHERIC RESEARCH - ATMOSPHERIC SCIENTISTS PUZZLE OVER HIGH-ALTITUDE FLASHES. *Science*, 264, 1250-1251.
- Mandelbrot, B. B. 1982. *The Fractal Geometry of Nature*. W. H. Freeman and Company.
- Marney, G. O. & K. Shanmugam. 1971. Effect of Channel Orientation on the Frequency Spectrum of lightning discharges. 4198-4202. *Journal of Geophysical Research*.
- Milikh, G. M., K. Papadopoulos & C. L. Chang (1995) ON THE PHYSICS OF HIGH-ALTITUDE LIGHTNING. *Geophysical Research Letters*, 22, 85-88.
- Niemeyer, L., L. Pietronero & H. J. Wiesmann (1984) FRACTAL DIMENSION OF DIELECTRIC-BREAKDOWN. *Physical Review Letters*, 52, 1033-1036.
- Papadopoulos, K., G. Milikh, A. Gurevich, A. Drobot & R. Shanny (1993) IONIZATION RATES FOR ATMOSPHERIC AND IONOSPHERIC BREAKDOWN. *Journal of Geophysical Research-Space Physics*, 98, 17593-17596.
- Pasko, V. P., U. S. Inan & T. F. Bell (1998) Spatial structure of sprites. *Geophysical Research Letters*, 25, 2123-2126.
- (2000) Fractal structure of sprites. *Geophysical Research Letters*, 27, 497-500.
- (2001) Mesosphere-troposphere coupling due to sprites. *Geophysical Research Letters*, 28, 3821-3824.
- Pasko, V. P., U. S. Inan, T. F. Bell & Y. N. Taranenko (1997) Sprites produced by quasi-electrostatic heating and ionization in the lower ionosphere. *Journal of Geophysical Research-Space Physics*, 102, 4529-4561.
- Pasko, V. P., M. A. Stanley, J. D. Mathews, U. S. Inan & T. G. Wood (2002) Electrical discharge from a thundercloud top to the lower ionosphere. *Nature*, 416, 152-154.
- Raiser, Y. P. 1997. *Gas Discharge Physics*. Berlin: Springer.
- Ramo, S. & J. R. Winnery. 1953. *Fields and Waves in Modern Radio*. John Wiley and Sons.
- Shumpert, T. H., M. A. Honnell & G. K. Lott. August 1982. Measured Spectral Amplitude of Lightning Sferics in the HF, VHF, and UHF Bands., 368-369. *IEEE Transactions on Electromagnetic Compatibility*.
- Taranenko, Y. N., U. S. Inan & T. F. Bell (1993a) INTERACTION WITH THE LOWER IONOSPHERE OF ELECTROMAGNETIC PULSES FROM LIGHTNING - HEATING, ATTACHMENT, AND IONIZATION. *Geophysical Research Letters*, 20, 1539-1542.
- (1993b) THE INTERACTION WITH THE LOWER IONOSPHERE OF ELECTROMAGNETIC PULSES FROM LIGHTNING - EXCITATION OF OPTICAL-EMISSIONS. *Geophysical Research Letters*, 20, 2675-2678.
- Tsang, K., K. Papadopoulos, A. Drobot, P. Vitello, T. Wallace & R. Shanny (1991) RF IONIZATION OF THE LOWER IONOSPHERE. *Radio Science*, 26, 1345-1360.
- Uman, M. 1987. *The Lightning Discharge*. NYC: Academic Press.
- Valdivia, J. A., G. M. Milikh & K. Papadopoulos (1998) Model of red sprites due to intracloud fractal lightning discharges. *Radio Science*, 33, 1655-1668.
- Vecchi, G., D. Labate & F. Canavero (1994) FRACTAL APPROACH TO LIGHTNING RADIATION ON A TORTUOUS CHANNEL. *Radio Science*, 29, 691-704.